Disorder and Proximity Driven Phenomena in s-Wave Superconductors

A Thesis Submitted
For the Degree of Master in Engineering

By

Naushad Ahmad Kamar

Theoretical Sciences Unit

Jawaharlal Nehru Centre For Advanced Scientific Research

Bangalore - 560 064

December 2013

Certificate

This is to certify that the thesis entitled "Disorder and Proximity Driven Phenomena in s-Wave Superconductors" being submitted to the Jawaharlal Nehru Centre For Advanced Scientific Research, Bangalore in partial fulfillment of the requirements for the award of the MS(Engg.) degree, embodies the research work done by Naushad Ahmad Kamar under my supervision at JNCASR, Bangalore. The work presented here is original and has not been submitted so far, in part or full, for any degree or diploma of any other university/institute.

_____

(Supervisor)

Declaration

I declare that the matter embodied in the thesis "Disorder and Proximity Driven Phenomena in s-Wave Superconductors" is carried out by me at the Theoretical Sciences Unit, Jawaharlal Nehru Centre for Advanced Scientific Research (JNCASR), Bangalore, India under the supervision of Prof. N. S. Vidhyadhiraja and it has not been submitted elsewhere for the award of any degree or diploma.

_____

Naushad Ahmad Kamar

Acknowledgements

Abstract

In this thesis, we have investigated two important issues in s-wave superconductors, namely effects of disorder and the proximity to normal metal on the superconducting state. The present thesis employs the framework of dynamical mean field theory (DMFT). We have developed extensions to the well-benchmarked impurity solver - iterated perturbation theory for superconductivity (IPTSC), and have used it within DMFT to study the above mentioned phenomena. The thesis has been divided into three chapters. Chapters two and three deal with effects of disorder on s-wave superconductors and chapter four deals with proximity of s-wave superconductor to normal metal. The three chapters are summarized below.

In Chapter 2, the disordered attractive Hubbard model is studied by combining dynamical mean field theory (DMFT), coherent potential approximation (CPA) and iterated perturbation for superconductivity (IPTSC) as an impurity solver. The disorder is modeled by taking random values of site-energies. We find that the superconducting order parameter (Φ) decreases with increasing disorder strength (x) and beyond a critical value of $x = x_c$, it completely vanishes, and system becomes non-superconducting. The spectral gap (E_g) shows non-monotonic behaviour. For weak x, E_g decreases with increasing x, and after a certain value of x, it increases with increasing x. Even after the destruction of superconductivity ($\Phi = 0$), the spectral gap persists, thus the system goes being a superconductor to an insulator with increasing disorder. We have calculated the phase diagram in interaction-disorder plane. It is found that x_c initially increases with increasing interaction (U), reaches a maximum and then decreases with increasing U. Thus superconductivity becomes less robust in presence of disorder.

In Chapter 3, we again investigate the disordered attractive Hubbard model with the same theoretical approach as in chapter-2, but with the difference that disorder is introduced in the on-site negative attraction, U. We assume that U is distributed according to a bimodal probability distribution, wherein an x fraction of sites are interacting ($U \neq 0$) and $(1 - x)$ fraction of sites are non-interacting ($U = 0$). it is found that the beyond a critical $x = x_c$, superconductivity is induced in the interacting as well as non-interacting sites. As a result, the whole system displays superconductivity. We find that x_c decreases with increasing U, thus interaction stabilizes the superconducting phase despite the presence

of disorder. From the results of the chapters 2 and 3, we can conclude that site disorder and interaction disorder have opposite effects.

In Chapter 4, we have studied the effects of proximity of a superconductor to a normal metal. The system is represented by a bilayer attractive Hubbard model using layer-DMFT and IPTSC as an impurity solver . We have considered one layer to be interacting ($U < 0$) and other layer to be non-interacting ($U = 0$). Both the layers are connected by an interplanar hopping ($t_\perp$). It is found that the superconductivity is induced ($\Phi \neq 0$) in the non-interacting layer. Beyond a certain value of value of $t_\perp$, both the interacting and non-interacting layers become non-superconducting.

Contents

List of Figures

Chapter 1

Introduction

1.1 Superconductivity

Superconductivity is a macroscopic quantum phenomenon characterised by complete disappearance of electrical resistance and expulsion of magnetic flux below a critical temperature. It was first discovered serendipitously in 1911 by H. Kamerlingh Onnes [1] in Leiden through the observation that the electrical resistance of mercury below a critical temperature ($T_c = 4.15$K) disappears. The expulsion of magnetic field or perfect diamagnetism was discovered almost two decades later and the phenomenon came to be known as the Meissner effect [2].

Superconductivity remained a great mystery for about four decades after its discovery. The discovery of the isotope effect provided one of the first breakthroughs by showing that the lattice vibrations namely phonons play a major role. In 1956 L. N. Cooper [3] showed theoretically that any attractive interaction, however small, can destabilise the Fermi surface. Combined with the works of many other, notably Frohlich, a consensus emerged that two electrons can bind through an attractive interaction that arises due to electron-phonon coupling [4] and form Cooper pairs, which may be represented roughly as bosons. These Cooper pairs can undergo Bose-Einstein condensation and result in superconductivity.

Motivated by these ideas, a microscopic theory of superconductivity was proposed by J. Bardeen, L. N. Cooper, and J. R. Schrieffer [5], which came to be known as the now famous BCS theory. Subsequent important work by Bogoliubov [6] and L. P. Gor'kov [7] led to the formulation of BCS theory

in the language of Green's functions. The BCS theory correctly explains most of the phenomena associated with conventional superconductors including the Meissner effect. The success of BCS theory is exemplified by the results shown in figure 1.1, which shows the close agreement of BCS theory predictions for the temperature dependence of the energy gaps with experimental measurements of In, Sn and Pb. In figure 1.1, the x axis represents the ratio of temperature to critical temperature (T/T_c) and the y axis represents the ratio of energy gap at temperature T to energy gap at zero temperature ($\varepsilon/\varepsilon_0$). In the BCS theory $\varepsilon/\varepsilon_0$ is related to T/T_c by the relation: $\varepsilon/\varepsilon_0 = \sqrt{(1 - T/T_c)}$, $\varepsilon_0 \simeq 3.5 k_B T_c$. It is seen that experimentally measured $\varepsilon/\varepsilon_0$ data of In, Sn, and Nb as a function of T/T_c collapses onto the universal BCS gap equation.
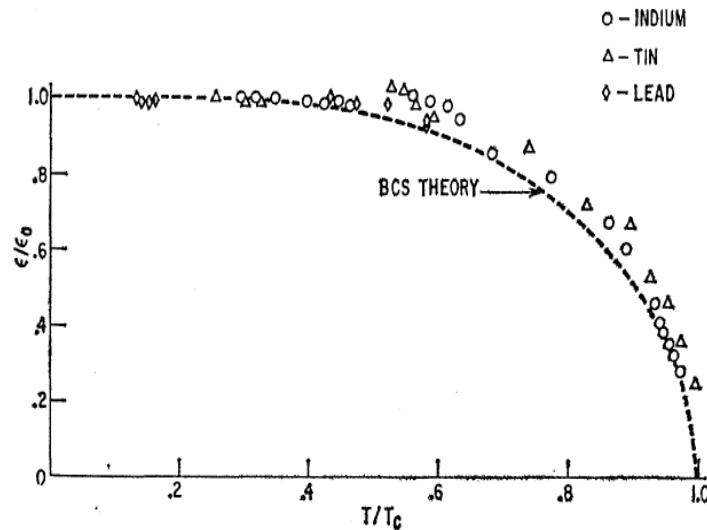
Figure 1.1: The energy gap of Pb, Sn and In films as function of reduced temperature compared with BCS theory (From Ref. [8]).

The superconducting state is characterized by a complex order parameter Φ, which describes the strength of superconductivity and the single particle spectral gap. There are two kind of superconductors, conventional (Nb, Pb, Sn, Hg, etc.) and unconventional ($CeCu_2Si_2, UPt_3, LaBaCuO_4$, etc.) superconductors. Conventional superconductors are those materials which are described by the BCS theory, and the pairing glue is provided by electron-phonon coupling. Unconventional superconductors exhibit strong deviations from the predictions of the BCS theory, in terms of unconventional

pairing mechanisms, exotic pairing symmetries and highly mysterious normal state properties.

One of the most demanding and challenging problems in condensed matter physics has been the interplay of disorder and correlation. Disorder drastically modifies the physical properties of electronic systems [9–11]. In 1958, Anderson showed theoretically [9] that disorder can localize electrons under certain conditions. Beyond a critical value of the disorder strength, x_c, and in absence of electron-electron interactions, a system can becomes insulating. Later, in a single parameter scaling theory by E. Abrahams, P. W. Anderson, D. C. Licciardello, and T. V. Ramakrishnan (popularly known as the gang of four) [12], it was proved that the value of x_c is zero for one and two-dimensional non-interacting systems. This was verified extensively through experiments. However, as always happens in science, contradiction to the established theory emerged, in the form of experiments by Kravchenko and collaborators, who demonstrated a metal to insulator transition experimentally [13] in two-dimensional systems. Theoretical work by Finkelstein and Punoose [14] established unambiguously that such a transition is indeed possible in two-dimensions and the scaling theory could become invalid because of the presence of electron-electron interactions. Thus a combination of correlations and disorder strongly modifies the properties of the materials.

In relation to the topic of superconductivity, the effects of disorder been extensively studied theoretically with different models and methods in the context of superconductor-insulator transition. But a complete picture of this transition has not emerged yet and unsolved issues remain like the nature of insulator, the mechanism of superconductor to insulator transition. There are many superconducting materials like, NbN [15–17], TiN [19], InO [18,20] that display superconductor to insulator transition. Early microscopic understanding of effects of non-magnetic disorder on superconductivity was given by Anderson [21] and Gor'kov [22]. It was proved that superconductivity is insensitive to disorder in the weak disorder limit. The strong disorder limit has been investigated theoretically in more recent times by different kinds of approaches [23–30]. Indeed, a disorder-induced superconductor to insulator transition has been seen in experimental studies as shown in figure 1.2 [16]. In figure 1.2, the x axis represents the temperature (T) and the y axis represents the dc resistivity (ρ). The Fermi wave vector is denoted by k_F, while l is the mean free path length, and the product $k_F l$ measures the strength of disorder ($k_F l < 1$ corresponds to strong disorder while large $k_F l$ corresponds to weak disorder). The superconducting critical temperature (T_c) decreases with increasing disorder strength, $T_c \rightarrow 0$ as

$k_F l \rightarrow 1$, and ρ decreases with increasing T, indicating a superconductor-insulator transition driven by disorder.
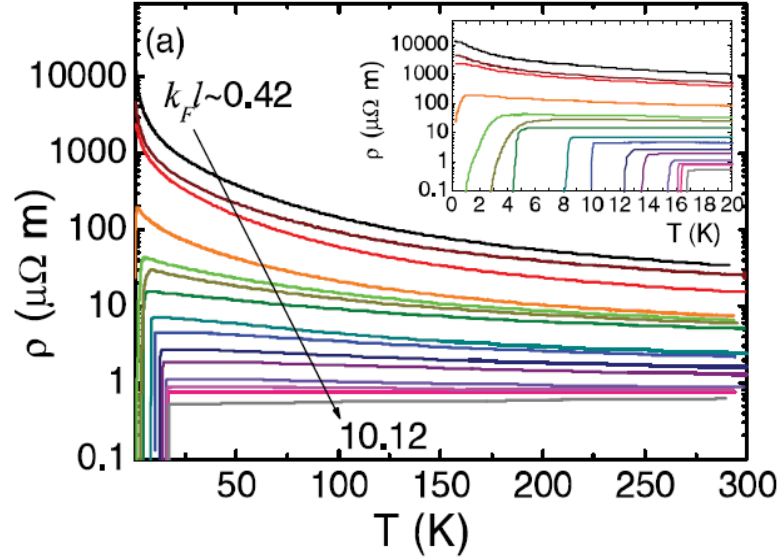
Figure 1.2: Resistivity vs temperature for NbN films for different values of $k_F l$, where k_F is Fermi wave vector and l is mean free path length. The parameter $k_F l$ characterizes the strength of disorder ($k_F l < 1$ corresponds to strong disorder while large $k_F l$ corresponds to weak disorder). (Figure is from Ref. [16]).

There are other situations wherein, superconductivity is induced because of doping one material with other. For example, PbTe is a semiconducting material which when doped with Tl displays superconductivity [31, 32]. It is observed that, beyond a critical value of doping (x_c) of Tl, the resistivity of $Pb_{1-x}Tl_x Te$ drops to zero at a finite critical temperature, thus indicating a superconducting ground state. Naturally, doping induces disorder, and so it has been proposed that $Pb_{1-x}Tl_x Te$ shows spatial distribution of negative interaction centers, that drives systems to a superconducting phase.

Superconductivity can be induced in a conventional metal or semiconductor not just by dopants as in the above example, but also by proximity to a superconductor. Cooper pairs from superconductor penetrate the normal metal layer and induce superconducting correlations in normal metal layer. The proximity of superconductor to metal has been investigated experimentally in layered systems such as Nb/Au [34, 35] and $NbSe_2$/Au [36], and the proximity of superconductor to ferromagnet has been studied in Nb/Fe [37–39], Nb/Gd [40, 41], V/Fe [42–44], $V/V_{1-x}Fe_x$ [45], Pb/Fe [46], Co/Al [47],

and $YBa_2Cu_3O_{7-\delta}/La_{0.7}Co_{0.3}MnO_3$ [48] etc. It has been found that the superconducting critical temperature decreases with increasing thickness of metal or ferromagnet.

In this thesis, we have investigated various aspects involving superconductivity such as the combined effect of disorder and correlations, induction of superconductivity due to negative-U centers and proximity effects. In the next section, we present an outline of the thesis.

1.2 Outline of the thesis

In Chapter 2, the disordered attractive Hubbard model is studied by combining dynamical mean field theory (DMFT) [49–51], coherent potential approximation (CPA) [52, 53] and iterated perturbation for superconductivity (IPTSC) [54] as an impurity solver. The disorder is modeled by taking random values of site-energies. We find that superconducting order parameter decreases (Φ^{CPA}) with increasing the disorder strength (x) and beyond a critical value of $x = x_c$, completely vanishes, and system becomes non-superconducting. The spectral gap shows non-monotonic behaviour. For weak x, it decreases with increasing x, and after a certain value of x, it increases with increasing x. After the destruction of superconductivity, the spectral gap persists, thus the system goes from superconductor to insulator. We have calculated the phase diagram in interaction-disorder plane. It is found that x_c first increases with increasing interaction (U), and then decreases with increasing U. Thus superconductivity becomes less robust in presence of disorder.

In Chapter 3, we again investigate the disordered attractive Hubbard model with the same theoretical approach as in the chapter-2, but with the difference that disorder is introduced in the on-site negative attraction, U. We assume that U is distributed according to a bimodal probability distribution, wherein an x fraction of sites are interacting ($U \neq 0$) and $(1 - x)$ fraction of sites are non-interacting ($U = 0$). it is found that the beyond a critical $x = x_c$, superconductivity is induced in the interacting as well as non-interacting sites. As a result, the whole system displays superconductivity. We find that x_c decreases with increasing U, thus interaction stabilizes the superconducting phase despite the presence of disorder. Thus, site disorder and interaction disorder have opposite effects.

In Chapter 4, we have studied the effects of proximity of a superconductor to a normal metal. The system is represented by a bilayer attractive Hubbard model using layer-DMFT and IPTSC as

an impurity solver . We have considered one layer to be interacting ($U < 0$) and other layer to be non-interacting ($U = 0$). Both the layers are connected by an interplanar hopping ($t_\perp$). It is found that the superconductivity is induced ($\Phi \neq 0$) in the non-interacting layer. Beyond a certain value of value of $t_\perp$, both the interacting and non-interacting layers become non-superconducting.

Bibliography

[1] H Kamerlingh Onnes 1911 Lieden Comm. **120b 122b 124c**.

[2] Meissner and Ochsenfeld 1933 Naturwissenschaften **21** 787.

[3] Cooper L N 1956 Phys. Rev. **104** 1189.

[4] Altland A and Simons B 2006 Cambridge University Press pp 190.

[5] Bardeen J, Cooper L N and Schrieffer J R 1957 Phys. Rev. **108** 1175.

[6] Bogolyubov N N 1958 Zh. Eksp. Teor. Fiz. **34** 58.

[7] Gor'kov L P 1958 Zh. Eksp. Teor. Fiz. **34** 735.

[8] Giaever I and Megerle K 1961 Phys. Rev. **122** 1101.

[9] Anderson P W 1958 Phys. Rev. **109** 1492.

[10] Lee P A and Ramakrishnan T V 1985 Rev. Mod. Phys. **57** 287.

[11] Belitz D and Kirkpatrick T R 1994 Rev. Mod. Phys. **66** 261.

[12] Abrahams E, Anderson P W, Licciardello D C and Ramakrishnan T V 1979 Phys. Rev. Lett. **42** 673.

[13] Kravchenko S V, Kravchenko G V, Furneaux J E, Pudalov V M and Iorio M D 1994 Phys. Rev. B **50** 8039.

[14] Punnoose A and Finkel'stein A M 2005 Science **310** 289.

[15] Mintu Mondal etal 2011 Phys. Rev. Lett. **106** 047001.

[16] Madhavi Chand *et. al* 2012 Phys. Rev. B **85** 014508.

[17] Mintu Mondal *et. al* 2013 Scientific Reports **3**, 1357 .

[18] Crane R *et. al* 2007 Phys. Rev. B **75** 184530.

[19] Benjamin Sacépé *et. al* 2010 Nature Communications **1** 140.

[20] Benjamin Sacépé *et. al* 2011 Nature Physics **7** 239-244.

[21] Anderson P W J 1959 Phys. Chem. Solids **11** 26.

[22] Abrikosov A A and Gor'kov L P 1959 Sov. Phys. JETP **9** 220.

[23] Ghosal A, Randeria M and Trivedi N 1998 Phys. Rev. Lett. **81** 3940-3943.

[24] Ghosal A, Randeria M and Trivedi N 2001 Phys. Rev. B **65** 014501.

[25] Yonatan Dubi, Yigal Meir and Yshai Avishai 2007 Nature **449** 876.

[26] Sanjeev Kumar and Prabuddha B Chakraborty 2013 arxiv:1302.1967.

[27] Trivedi N, Scalettar R T and Randeria M 1996 Phys. Rev. B **54** R3756.

[28] Scalettar R T, Trivedi N and Huscroft C 1999 Phys. Rev. B **59** 4364.

[29] Karim Bouadim, Yen Lee Loh, Mohit Randeria and Nandini Trivedi 2011 Nature Physics **7** 884-889.

[30] Feigel'man M V, Ioffe L B, Kravtsov V E and Yuzbashyan E A 2007 Phys. Rev. Lett. **98** 027001.

[31] Matsushita Y etal 2005 Phys. Rev. Lett. **94** 157002 .

[32] Matsushita Y etal 2006 Phys. Rev. B **74** 134512 .

[33] Andreev A F 1964 Zh. Eksp. Teor. Fiz. **46** 1823.

[34] Jinho Kim, Yong-Joo Doh, K. Char, Hyeonjin Doh, Han-Yong Choi 2005 Phys. Rev. B **71** 214519.

[35] Hiroki Yamazaki, Nic Shannon and Hidenori Takagi 2006 Phys. Rev. B **73** 094507.

[36] Truscott A D, Dynes R C and Schneemeyer L F 1999 Phys. Rev. Lett. **83** 1014-1017.

[37] Kawaguchi K and Sohma M 1992 Phys. Rev. B **46** 14722.

[38] Verbanck G, Potter C D, Metlushko V, Schad R, Mosh-chalkov V V and Bruynseraede Y 1998 Phys. Rev. B **57** 6029.

[39] Mühge Th, Theis-Bröhl K, Westerholt K, Zabel H, Garif'yanov N N, Goryunov Yu V, Gari-fullin I A and Kha-liullin G G 1998 Phys. Rev. B **57** 5071.

[40] Strunk C, Sürgers C, Paschen U and Löhneysen H V 1994 Phys. Rev. B **49** 4053.

[41] Jiang J S, Davidovic D, Daniel H Reich and Chien C L 1995 Phys. Rev. Lett. **74** 314.

[42] Wong H K, Jin B Y, Yang H Q, Ketterson J B and Hilliard J E 1986 J. Low Temp. Phys. **63** 307.

[43] Koorevaar P, Suzuki Y, Coehoorn R and Aarts J 1994 Phys. Rev. B **49** 441.

[44] Tagirov L R, Garifullin I A, Garif'yanov N N, Khle-bnikov S Ya , Tikhonov D A, Westerholt K and Zabel H 2002 J. Magn. Magn. Mater. **240** 577.

[45] Aarts J, Geers J M E, Brück E, Golubov A A and Coe-hoorn R 1997 Phys. Rev. B **56** 2779.

[46] Lazar L, Westerholt K, Zabel H, Tagirov L R, Goryunov Yu V, Garifyanov N N and Garifullin I A 2000 Phys. Rev. B **61** 3711.

[47] Goto H 2003 Physica B **329-333** 1425.

[48] Sefrioui Z, Arias D, Peña V, Villegas J E, Varela M, Prieto P, Leòn C, Martinez J L and Santa-maria J 2003 Phys. Rev. B **67** 214511.

[49] Georges A, Kotliar G, Krauth W and Rozenberg M J 1996 Rev. Mod. Phys. **68** 13.

[50] Kotliar G and Vollhardt D 2004 Physics Today **57** 53-59.

[51] Vollhardt D 2010 AIP Conference Proceedings **1297**, 339.

[52] Elliott R J, Krumhansl J A and Leath P L 1974 Rev. Mod. Phys. **46** 465.

[53] Janiš V and Vollhardt D 1992 Phys. Rev. B **46** 15712.

[54] Garg A, Krishnamurthy H R and Randeria M 2005 Phys. Rev. B **72** 024517.

Chapter 2

Site-disorder driven superconductor to insulator transition

2.1 Introduction

The combined effect of disorder and correlations on the superconducting state has been extensively studied since many decades but a complete picture has not emerged yet [1, 2]. Many recent experimental studies of disordered superconducting thin films have investigated the superconductor-insulator transition (SIT) [3–8]. In disordered NbN s-wave superconductors [3–5], an SIT was observed through scanning tunneling spectroscopy and penetration depth measurements. The effective disorder in NbN, given by the product of Fermi wave vector (k_F) and electronic mean free path (l), is introduced by controlling the vacancy of Nb atoms. The insulating state at large disorder has been a subject of debate. Finite frequency measurements of superfluid stiffness [6] have indicated the existence of a Bose insulator state with localized Cooper pairs. However, a better understanding of the SIT and the associated insulating state in the large disorder limit requires more theoretical scrutiny.

Localized Cooper pairs indicate a system with local attractive interactions, which are most appropriately represented by the attractive Hubbard model (AHM) [9]. The study of dirty superconductors can thus be naturally carried out by investigating the effect of disorder in the attractive Hubbard model. The clean limit of the AHM has been extensively studied using Bogoliubov-de Gennes type mean field (BdGMF) theories and more recently using iterated perturbation theory with superconduct-

ing bath (IPTSC) [10], numerical renormalization group (NRG) [11] and continuous time quantum Monte Carlo (CTQMC) [12] within dynamical mean field theory (DMFT) [13–15]. The main issue that has been focused on is the BCS-BEC crossover for different fillings and interaction strengths. Very recently, a statistical-DMFT study of the Bethe lattice disordered AHM has been carried out [16].

The systems investigated experimentally, such as NbN_x [3–5], InO_x [6, 8] and TiN_x [7] are in the strong disorder limit, wherein the early theories of dirty superconductors, e.g by Anderson [17] and by Abrikosov and Gor'kov [18] are not really applicable. Hence a proper theoretical approach is needed which treats the effects of strong attractive interactions and disorder on an equal footing. One such method, namely the BdGMF has been employed to investigate the AHM with site [19–21] as well as bond disorder [22]. However, the method, being based on a mean field approximation, albeit inhomogeneous, has limitations in terms of not incorporating quantum fluctuations. Recent NRG [11] calculations of the clean AHM also point out several deficiencies of the BdGMF method. Beyond mean field, QMC [23–25] studies of finite size lattices have validated the decrease of superconducting order parameter (Φ) with increasing disorder, but due to finite size effects, a complete destruction of Φ at large disorder could not be seen. However, with increasing temperature, a superconductor-insulator transition was observed in the dc conductivity calculations.

In this work, we carry out a detailed study of the disordered AHM by combining coherent potential approximation(CPA) [26, 27], with DMFT and iterated perturbation theory for superconductivity(IPTSC) [10]. The IPTSC solver has the advantage over methods such as QMC of obtaining real frequency spectra at zero temperature and in the thermodynamic limit, while being computationally inexpensive. The reliability of our approach is enhanced by the fact that the IPTSC is known to benchmark well with NRG results for the clean AHM [11]. To distinguish between dynamical and static effects, we have also carried out BdGMF studies within CPA+DMFT. As anticipated by the previous inhomogeneous mean field and QMC calculations, we find a SIT with increasing disorder. We map out the detailed behaviour of the SIT in the disorder-interaction plane. We also investigate the distribution of the local order parameter, and point out that some of the subtle aspects of the experimentally observed SIT require an extension of single-site DMFT through e.g the statistical DMFT or cluster extensions such as the dynamical cluster approximation. This chapter is structured as follows: In the following section, we outline the model and the formalism used. Next, we present our results for the

local order parameter, the spectra, the distribution of the order parameter and the phase diagram. We conclude in the final section.

2.2 Model and formalism

The attractive Hubbard model (AHM) is expressed, in standard second quantized notation by the following Hamiltonian:

$$\mathcal{H} = \sum_{i\sigma} \varepsilon_i c_{i\sigma}^\dagger c_{i\sigma} - t \sum_{\langle ij\sigma \rangle} \left(c_{i\sigma}^\dagger c_{j\sigma} + h.c \right) - |U| \sum_i n_{i\uparrow} n_{i\downarrow} - \mu \sum_{i\sigma} c_{i\sigma}^\dagger c_{i\sigma} \tag{2.1}$$

where $c_{i\sigma}$ annihilates an electron on i^{th} lattice site with spin σ, and $n_{i\sigma} = c_{i\sigma}^\dagger c_{i\sigma}$; t is nearest-neighbour hopping amplitude, ε_i is site-energy, and μ is chemical potential. The disorder is represented by randomness in site energies, which we choose to be distributed according to a uniform probability distribution function $P_\varepsilon(\varepsilon_i)$,

$$P_\varepsilon(\varepsilon_i) = \frac{\Theta(\frac{x}{2} - |\varepsilon_i|)}{x} \tag{2.2}$$

where x is disorder strength in unit of $t \, (= 1.0)$.

The CPA in conjunction with DMFT is the best single-site approach to study the interplay of disorder with interactions in strongly correlated systems [32]. To investigate the effects of disorder on the superconducting state, we employ the best single-site quantum approaches, namely DMFT in conjunction with CPA. Within DMFT, the lattice model is mapped onto a single-impurity model embedded in a self-consistently determined bath. For the present problem, the effective medium is in a superconducting state, hence the Nambu formalism must be used. The effective action [13] (derived in appendix A.5) for a given site i within DMFT in Nambu formalism is given by

$$S_{eff}(i) = - \int_0^\beta d\tau_1 \int_0^\beta d\tau_2 \Psi_i^\dagger(\tau_1) \hat{\mathscr{G}}^{i\,-1}(\tau_1 - \tau_2) \Psi_i(\tau_2) - |U| \int_0^\beta d\tau n_{i\uparrow}(\tau) n_{i\downarrow}(\tau) \tag{2.3}$$

where $\Psi_i(\tau)$, the two component Nambu's spinor and $\hat{\mathscr{G}}^i$, the host Green's function in Nambu for-

malism are given by

$$\Psi_i(\tau) = \begin{bmatrix} c_{i\uparrow}(\tau) \\ c_{i\downarrow}^{\dagger}(\tau) \end{bmatrix}$$

and

$$\mathscr{G}^i(\omega) = \begin{bmatrix} \omega^+ - \varepsilon_i + \mu - \Delta_{11}(\omega) & -\Delta_{12}(\omega) \\ -\Delta_{21}(\omega) & \omega^+ + \varepsilon_i - \mu - \Delta_{22}(\omega) \end{bmatrix}^{-1}. \tag{2.4}$$

The impurity Green's function in Nambu formalism is given as

$$\hat{G}^i(\tau) = -\langle T_\tau \Psi_i(\tau)\Psi_i^{\dagger}(0)\rangle$$

$$\hat{G}^i(\omega) = \begin{bmatrix} \gamma_i(\omega) - \Delta_{11}(\omega) & -\Delta_{12}(\omega) - S_i(\omega) \\ -\Delta_{21}(\omega) - S_i(\omega) & -\gamma_i^*(-\omega) - \Delta_{22}(\omega) \end{bmatrix}^{-1} \tag{2.5}$$

where $\Delta_{\alpha\beta}$, $\alpha, \beta = 1, 2$ are components of the disorder-averaged hybridisation function matrix $\hat{\Delta}$; $\gamma(\omega) = \omega^+ + \mu - \varepsilon_i - \Sigma_i(\omega)$; Σ_i and S_i are normal and anomalous self-energies of the ith site respectively.

To calculate the local self-energies, $\Sigma_i(\omega^+)$ and $S_i(\omega^+)$ for the ith site, we use iterated perturbation theory for superconductivity (IPTSC) [10] as the impurity solver. In the IPTSC method, based on second order perturbation theory, the self-energies(second order self-energies are derived in appendix A.1 and A.2.) are given by the following ansatz:

$$\Sigma_i(\omega^+) = -U\frac{n_i}{2} + A_i\Sigma_i^{(2)}(\omega^+) \tag{2.6}$$

$$S_i(\omega^+) = -U\Phi_i + A_iS_i^{(2)}(\omega^+) \tag{2.7}$$

where the local filling n_i and order parameter Φ_i are given by

$$n_i = -\frac{2}{\pi}\int_{-\infty}^{\infty} d\omega \, \text{Im}(G_{11}^i(\omega^+))f(\omega) \tag{2.8}$$

$$\Phi_i = \int_{-\infty}^{\infty} d\omega \frac{-\text{Im}(G_{12}^i(\omega^+))}{\pi}f(\omega) \tag{2.9}$$

14

and $f(\omega) = \theta(-\omega)$ is the Fermi-Dirac distribution function at zero temperature. In the ansatz above (equations (2.6 and 2.7)), the second order self-energies are given by

$$\Sigma_i^{(2)}(\omega^+) = U^2 \int_{-\infty}^{\infty} \prod_{j=1}^{3} d\omega_j \frac{g_{1i}(\omega_1, \omega_2, \omega_3)N(\omega_1, \omega_2, \omega_3)}{\omega^+ - \omega_1 + \omega_2 - \omega_3}$$

and

$$S_i^{(2)}(\omega^+) = U^2 \int_{-\infty}^{\infty} \prod_{j=1}^{3} d\omega_j \frac{g_{2i}(\omega_1, \omega_2, \omega_3)N(\omega_1, \omega_2, \omega_3)}{\omega^+ - \omega_1 + \omega_2 - \omega_3}, \tag{2.10}$$

where

$$N(\omega_1, \omega_2, \omega_3) = f(\omega_1)f(-\omega_2)f(\omega_3) + f(-\omega_1)f(\omega_2)f(-\omega_3)$$

$$g_{1i}(\omega_1, \omega_2, \omega_3) = \tilde{\rho}_{11}^i(\omega_1)\tilde{\rho}_{22}^i(\omega_2)\tilde{\rho}_{22}^i(\omega_3) - \tilde{\rho}_{12}^i(\omega_1)\tilde{\rho}_{22}^i(\omega_2)\tilde{\rho}_{12}^i(\omega_3)$$

$$g_{2i}(\omega_1, \omega_2, \omega_3) = \tilde{\rho}_{12}^i(\omega_1)\tilde{\rho}_{12}^i(\omega_2)\tilde{\rho}_{12}^i(\omega_3) - \tilde{\rho}_{11}^i(\omega_1)\tilde{\rho}_{12}^i(\omega_2)\tilde{\rho}_{22}^i(\omega_3) \tag{2.11}$$

and the spectral functions $\tilde{\rho}_{\alpha\beta}^i, \alpha, \beta = 1, 2$ are given by the imaginary part of the 'Hartree-corrected' host Green's function, namely $\hat{\tilde{\rho}}_i = -\mathrm{Im}\hat{\mathscr{G}}^i/\pi$. The latter is given by

$$\hat{\mathscr{G}}^i(\omega) = \begin{bmatrix} \omega^+ + \mu - \varepsilon_i - \Delta_{11}(\omega) + U\frac{n_i}{2} & -\Delta_{12}(\omega) + U\Phi_i \\ -\Delta_{21}(\omega) + U\Phi_i & \omega^+ - \mu + \varepsilon_i - \Delta_{22}(\omega) - U\frac{n_i}{2} \end{bmatrix}^{-1} \tag{2.12}$$

Finally the coefficient A_i (derive in appendix A.4) in the IPTSC ansatz (equations (2.6 and 2.7) which is determined by the high frequency limit, is given by

$$A_i = \frac{\frac{n_i}{2}\left(1 - \frac{n_i}{2}\right) - \Phi_i^2}{\frac{n_{0i}}{2}\left(1 - \frac{n_{0i}}{2}\right) - \Phi_{0i}^2}, \tag{2.13}$$

where the pseudo order-parameter Φ_{0i} and the pseudo occupancy n_{0i} are given by

$$n_{0i} = 2\int_{-\infty}^{\infty} d\omega\, \tilde{\rho}_{11}^i(\omega)f(\omega)$$

$$\text{and} \quad \Phi_{0i} = \int_{-\infty}^{\infty} d\omega\, \tilde{\rho}_{12}^i(\omega)f(\omega) \tag{2.14}$$

Using the coherent potential approximation (CPA) for incorporating disorder, the CPA Green's

function is given by an arithmetic averaging over local Green's functions as

$$\hat{G}^{CPA}(\omega) = \int_{\frac{-x}{2}}^{\frac{x}{2}} d\varepsilon_i \hat{G}^i(\omega;\varepsilon_i) P_\varepsilon(\varepsilon_i). \tag{2.15}$$

Since the CPA maps the disordered problem onto a translationally invariant problem, a lattice Green's function may then be defined as

$$\hat{G}_{latt}(\vec{k},\omega) = \begin{bmatrix} \omega^+ + \mu - \varepsilon(\vec{k}) - \Sigma_{11}^{CPA}(\omega) & -\Sigma_{12}^{CPA}(\omega) \\ -\Sigma_{21}^{CPA}(\omega) & \omega^+ - \mu + \varepsilon(\vec{k}) - \Sigma_{22}^{CPA}(\omega) \end{bmatrix}^{-1} \tag{2.16}$$

where the self-consistency condition is that the lattice self-energy is the same as the CPA self-energy, hence the CPA Green's function in term of average self-energy is given as

$$\hat{G}^{CPA}(\omega) = \begin{bmatrix} \omega^+ + \mu - \Delta_{11}(\omega) - \Sigma_{11}^{CPA}(\omega) & -\Delta_{12}(\omega) - \Sigma_{12}^{CPA}(\omega) \\ -\Delta_{21}(\omega) - \Sigma_{21}^{CPA}(\omega) & \omega^+ - \mu - \Delta_{22}(\omega) - \Sigma_{22}^{CPA}(\omega) \end{bmatrix}^{-1} \tag{2.17}$$

The equations are closed by observing that the $\vec{k}$ summed lattice Green's function should be the CPA Green's function, i.e

$$\frac{1}{N_s} \sum_{\vec{k}} \hat{G}_{latt}(\vec{k},\omega) = \hat{G}^{CPA}(\omega)$$

which may be converted to a density of states integral and hence expressed as

$$\int_{-\infty}^{\infty} d\varepsilon \rho_0(\varepsilon) \hat{G}_{latt}(\varepsilon,\omega) = \hat{G}^{CPA}(\omega), \tag{2.18}$$

where N_s and $\rho_0(\varepsilon)$ are number of lattice sites and non-interacting density of states respectively.

2.3 Numerical Algorithm

In practice, we follow the steps outlined below to obtain the converged order parameter and spectra.

1. Guess a hybridisation matrix $\hat{\Delta}(\omega)$ and n_i, Φ_i for each site. In practice, we choose either a previously converged solution or the non-interacting $\hat{\Delta}(\omega)$ with $n_i = 1$ and $\Phi_i = 1/2 \; \forall \, i$.

2. Given a hybridization, occupancy and order parameter, use equation (2.12) to calculate the host Green's function matrix, $\hat{\mathscr{G}}^i(\omega)$.

3. From equation (2.14) , calculate pseudo-occupancy and pseudo-order parameter, n_{0i} and Φ_{0i}.

4. Now by using equations (2.6, 2.7, 2.10, 2.11, and 2.13) calculate the regular and anomalous self-energies, $\Sigma_i(\omega)$ and $S_i(\omega)$.

5. Then by using equations (2.5, 2.8, and 2.9) calculate impurity Green's function $\hat{G}^i(\omega)$, n_i, Φ_i for each site.

6. The disorder-averaged Green's function, $\hat{G}^{CPA}(\omega)$ is obtained using equation (2.15).

7. We consider the AHM on Bethe lattice of infinite connectivity at half filling, which is achieved by setting $\mu = -U/2$. For Bethe lattice the self-consistency condition is simply given by

$$\hat{\Delta}(\omega) = \frac{t^2 \sigma_z \hat{G}^{CPA}(\omega)\sigma_z}{4} \tag{2.19}$$

where σ_z is z component of Pauli's matrix. Using equation (2.19), a new hybridisation matrix $\hat{\Delta}$ is obtained.

8. If the hybridisation matrix $\hat{\Delta}(\omega)$ from step 7 and n_i, Φ_i from step 5 are equal (within a desired numerical tolerance) to the guess hybridisation matrix $\hat{\Delta}(\omega)$, n_i and Φ_i from step 1, then the iterations may be stopped, else the iterations continue until desired convergence is achieved.

The results obtained using the above-mentioned procedure will be denoted as IPTSC. We have also carried out mean-field calculations by 'turning off' the dynamical self-energies in equations 2.6 and 2.7. These results will be denoted as BdGMF. We present our results in the next section.

2.4   Parallel Implementation

In figure 2.1, parallel implementation of above numerical algorithm is shown. To parallelize above numerical algorithm, we have used message passing interface (MPI). Each square box represents a

processor. In this chapter, we have considered 1600 impurities, and the calculation is performed on 16 processors Thus in each processor, 100 impurities are solved, and averaging is done in root processor (processor number 1).

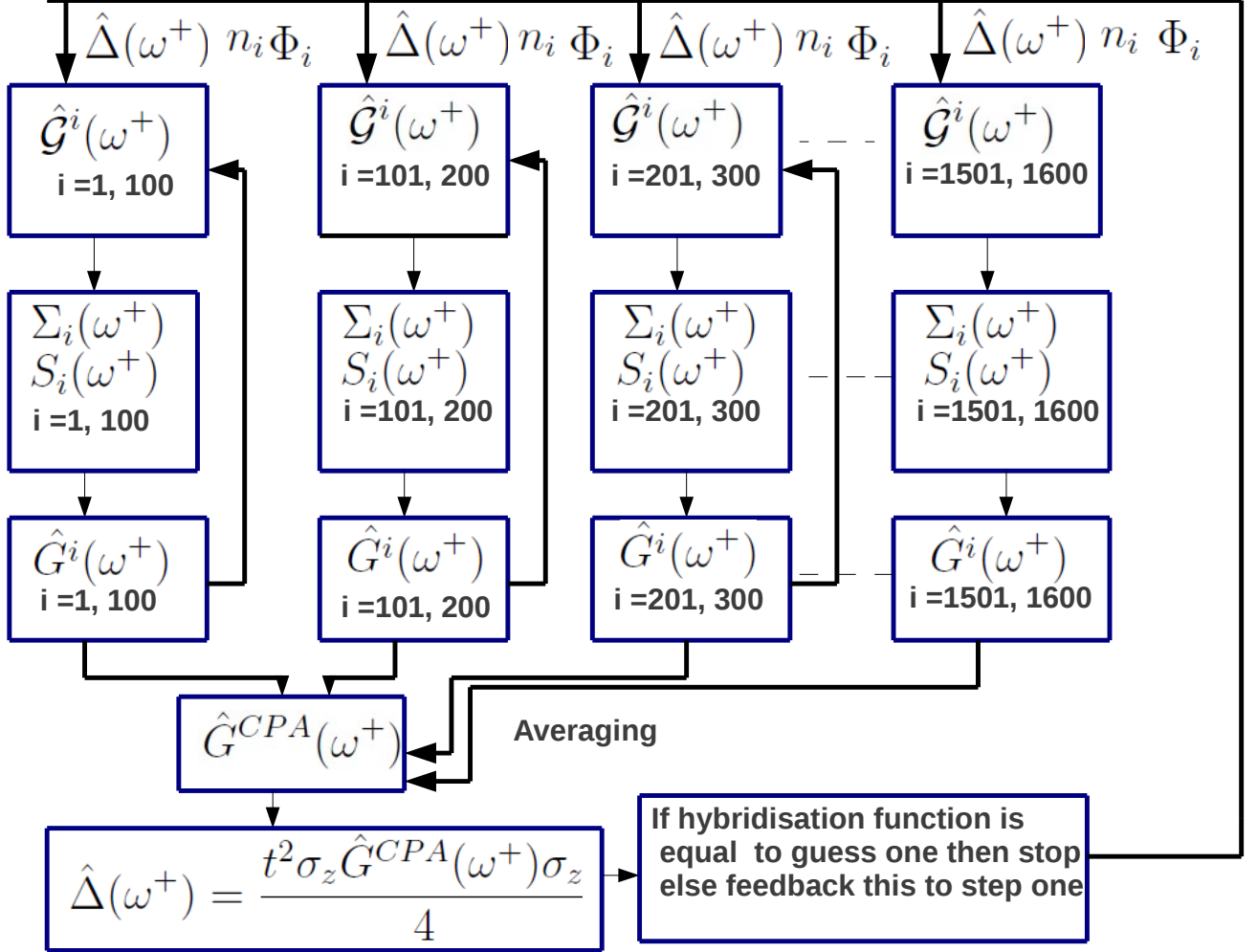Figure 2.1: Parallel implementation of above numerical algorithm

2.5 Results and discussion

A recent study of the clean AHM ($x = 0$) has shown that results obtained using the numerically exact NRG [11] compare well with those from the approximate IPTSC method, thus indicating its reliability for the present problem. A total of 1600 lattice sites have been considered in our calculations. This

implies that the impurity problem needs to be solved 1600 times for each DMFT iteration. A fully parallel implementation allows us to carry out efficient calculations in a wide-parameter range. This must be contrasted with previous state-of-the-art QMC calculations which have been carried out on a 8×8 square lattice, and results have been obtained at finite temperature on the imaginary frequency Matsubara axis. Thus not only are we able to consider much larger lattice sizes than previous works, but also obtain real frequency spectra directly at zero temperature.

We review the physics of the clean AHM within DMFT briefly. At half-filling ($n = 1$), it is well known that the AHM has two instabilities, namely superconductivity and charge-density wave (CDW). If the CDW instability is ignored, then the superconducting order parameter (Φ) becomes non-zero only for $U > U_{c1}$. The ground state is a normal metal for low interactions, while for $U > U_{c1}$, the single-particle spectrum develops a BCS superconducting gap. It is known from NRG calculations, that agree very well with IPTSC results, that with increasing U, the order parameter increases and saturates to a finite value as $U \to \infty$. However, more recent CTQMC based calculations [12] at a fixed finite temperature show that at large U, the order parameter decreases again, and vanishes beyond a certain $U = U_{c2}$. In this work, since we have carried out zero temperature calculations, we will choose to take the NRG results as our benchmark.

2.5.1 Varying disorder; fixed interaction strength

In the clean case, the half-filling condition is maintained by choosing $\varepsilon_i = 0$ and $\mu = -U/2$. For $x > 0$ the half-filling condition is again maintained through $\mu = -U/2$. The individual sites have site-energies that are distributed uniformly over $[-x/2, x/2]$, so there is very little probability that any single-site would have exactly $\varepsilon_i = 0$. This implies that for a disordered AHM at a global half-filling condition, the individual sites are away from half-filling, hence the CDW instability need not be considered. In figure 2.2 we show the diagonal spectral function as a function of frequency for different values of disorder at a fixed interaction strength, namely $U = 2$. The panel (a) represents results for lower disorder ($x \leq 0.5$), while the panel (b) represents higher disorder ($x \geq 0.5$). The zero disorder case in the panel (a) represents the clean AHM result. The system has a superconducting gap E_g. Flanking the band edges are the sharp 'coherence peaks'. With increasing disorder, the coherence peaks melt and change into broad features. The insets show an expanded view of the low frequency
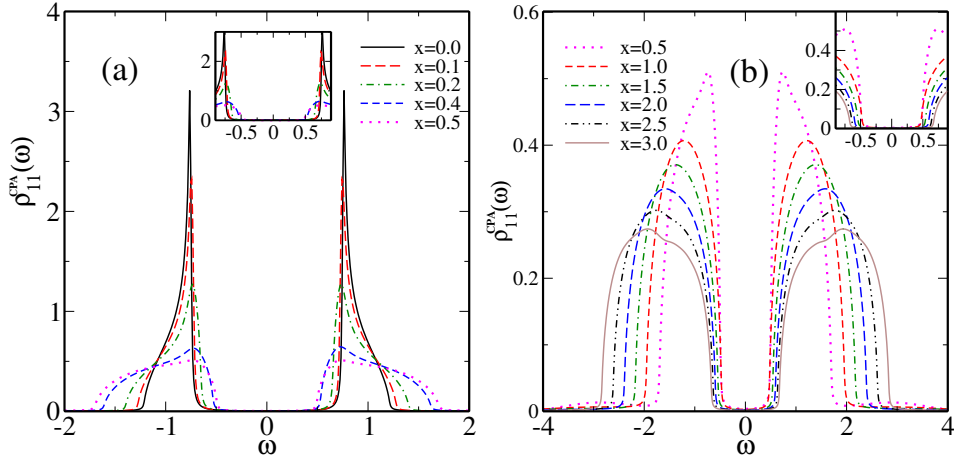
Figure 2.2: (color online) Diagonal spectral function as function of frequency for different values of x at U=2.0: (a) low disorder results ($0 < x \leq 0.5$); (b) strong disorder results ($x \geq 0.5$). Insets show an expanded view of the low frequency gap region.

gap region.
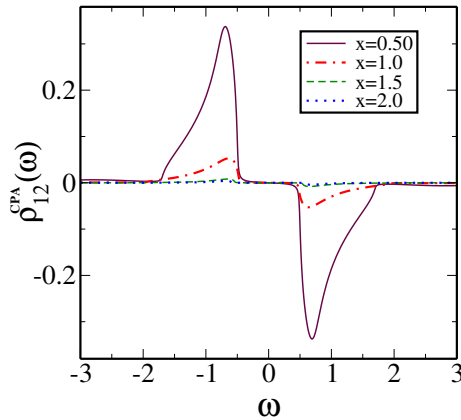
Figure 2.3: Off diagonal spectral function for different values of x at a fixed $U = 2.0$.

To understand the nature of the gap, we need to analyse the off-diagonal spectral function. These are shown in figure 2.3, for disorder values varying from $x = 0.5$ to $x = 2$, and $U = 2$. It is seen clearly that the entire spectral weight decreases rapidly with increasing x, and finally goes to zero at $x \sim 1.5$. Comparing with figure 2.2, we see that the spectral gap does not close for any x. Thus, the system exhibits a superconductor-insulator transition (SIT) as a function of increasing disorder at a fixed U.

The effective averaged s-wave pairing amplitude, Φ^{CPA} is defined as

$$\Phi^{CPA} = \int_{-\infty}^{\infty} d\omega \frac{-\mathrm{Im}(G_{12}^{CPA}(\omega^+))f(\omega)}{\pi}, \qquad (2.20)$$

and computed using the mean field (dashed line) and IPTSC (solid line) methods for a fixed interaction strength. In figure 2.4, we show the spectral gap and the disorder-averaged superconducting order
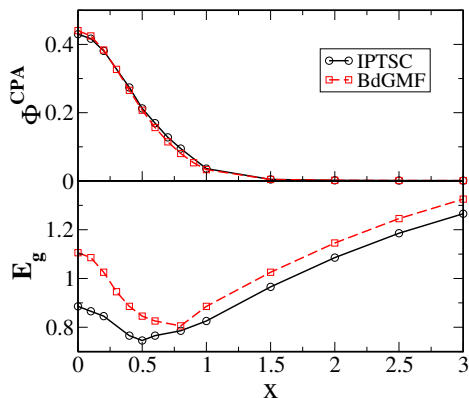
Figure 2.4: Top panel: The disorder-averaged superconducting order parameter (solid line) as a function of x at $U = 2.0$. The dashed line is the BdGMF result for comparison. Bottom panel: The spectral gap as a function of disorder.

parameter as a function of disorder in the bottom and top panels respectively. It is observed that the gap decreases, reaches a minimum, and then increases with increasing disorder. This kind of behaviour of spectral gap with disorder is reported in [19, 20, 22] . A theoretical investigation based on fractal nature of wave function also confirms the increase in spectral gap with disorder [28]. The order parameter, in contrast to the gap, decreases monotonically with increasing disorder and vanishes beyond $x \sim 1.5$. This result, which states that the superconducting state is destroyed beyond a critical disorder strength is consistent with previous QMC results, although the latter were obtained through extrapolation for finite size lattices. We show the BdGMF(CPA) result (dashed line) also in the same figure, and it is seen that the mean-field result and the full DMFT result hardly differ, indicating that local quantum fluctuations are not playing a significant role in the destruction of the superconducting state. Since the order parameter is finite for $x \lesssim 1.5$, the spectral gap is a superconducting gap, while for higher disorder ($x > 1.5$), since $\Phi = 0$, E_g represents an insulating gap. We also show the BdGMF(CPA) results for Φ and E_g in the same figure. It is seen that the spectral gap is overestimated

21

by the static mean field approach for finite disorder, as was found at $x = 0$ [10].

The dependence of the gap on x is non-monotonic, and deserves some attention. For weak disorder, the gap decreases with increasing x, and this may be understood through the clean AHM. For $x = 0$, the spectral gap becomes smaller and asymmetric (about the chemical potential), with either increasing or decreasing the filling away from 1 [12]. Thus, we expect that with increasing disorder, since most sites would be off-half-filling, the spectral gap within CPA, arising as the arithmetic mean of the individual spectra, would decrease for weak disorder. The preceding argument assumes that the hybridization remains largely unaffected, which is true for weak disorder. However, for moderate and large disorder, the hybridization gets modified strongly, and the simple arithmetic averaging result cannot be used to understand the increase in gap at larger disorder values ($x \gtrsim 1.5$). In order to understand the behaviour at large disorder, we will need to probe the distribution of the order parameter and gap over all the sites in the lattice. This is considered next.
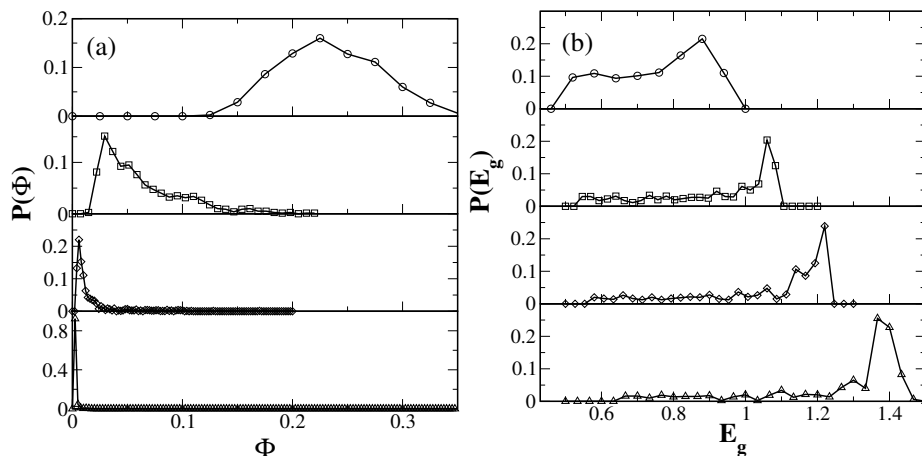
Figure 2.5: Probability distribution of (a) local superconducting order parameter and (b) spectral gap for different values of $x = 0.5, 1.0, 1.5, 2.0$ (from top to bottom) at $U = 2.0$.

In figure 2.5(a), the probability distribution function of local superconducting order parameter (PDF-OP) for different values of x is shown. For small disorder, the PDF-OP is broad, and peaked moderately at a certain typical value of Φ. With increasing x the typical Φ decreases sharply and the PDF-OP narrows down considerably. This indicates that, while in the weak disorder limit, arithmetic averaging may be used, in the strong disorder limit the typical value will manifest macroscopically. This is also reflected in the probability distribution function for spectral gap (PDF-SG). As expected,

the PDF-SG is also broad at weak disorder and narrows considerably at large disorder. In fact, since the weight contained in the peak is almost more than 50%, most of the sites will have a gap in the neighbourhood of the gap value corresponding to the peak. Since the peak occurs at higher values of the gap with increasing x, the gap in the CPA spectral function, shown in the bottom panel of figure 2.4, increases with increasing x. In previous literature based on BdGMF or QMC of finite lattices incorporating inhomogeneous order parameters, this increase in gap as a function of x has been attributed to decrease in localization length. Our results are based on the CPA, which is known to ignore localization effects. Thus we suggest that the arguments based on PDF are sufficient, and localization physics need not be invoked to explain the increase of the insulating gap. A more sophisticated treatment of this problem could be through typical medium theory, and subsequently statistical DMFT. Although the latter has been carried out [16], this specific issue has not been addressed.

2.5.2 Fixed disorder; varying interaction strength
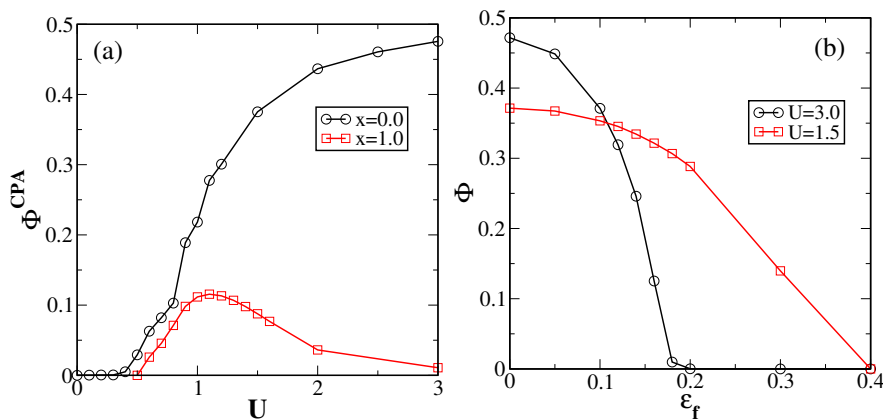
Figure 2.6: (a) Superconducting order parameter of the disordered AHM as a function of U at $x = 0, 1.0$; (b) The Φ of the clean AHM as a function of site-energy ε_f for fixed $U = 1.5$ and 3.0.

We have considered the behaviour of physical quantities as a function of disorder at a fixed interaction strength. Now, we show the order parameter as a function of U at a fixed disorder. In the figure 2.6(a), the superconducting order parameter computed at $x = 0$ and $x = 1.0$ is shown as a function of U. For the clean case ($x = 0$), as mentioned before, Φ increases and eventually saturates with increasing U. However, at finite disorder, Φ^{CPA} increases, reaches a maximum and subsequently decreases. Thus when we turn on disorder, the order parameter dependence on U changes qualitatively.

This can again be understood very simply from the clean AHM result, that at a fixed U, Φ decreases with increasing particle-hole asymmetry defined by $\eta = 1 - 2|(\varepsilon_i - \mu)/U|$, as shown in figure 2.6(b). For a larger U, the decrease of Φ with increasing η is much more rapid. Increasing site-disorder implies creating a greater number of sites with large η, which would have a smaller Φ as compared to the sites with $\eta \sim 0$. Thus, with increasing interaction strength, and a fixed disorder concentration, the superconducting order parameter should decrease, and is indeed obtained.

2.5.3 'Phase diagram'
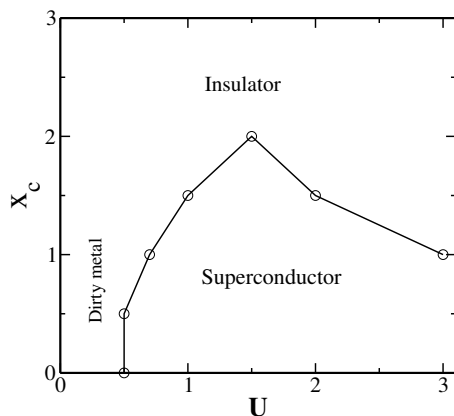
Figure 2.7: The critical disorder $x_c(U)$ beyond which the superconducting state is completely destroyed is shown as a function of U.

The variation of the spectral gap and the superconducting order parameter, shown in figure 2.4, was for a specific interaction strength, namely $U = 2.0$. We have repeated our calculations for various other U values, and could thus find the critical disorder strength $x_c(U)$, beyond which the superconducting state is completely destroyed. As shown in figure 2.7, we find that for large U, the $x_c(U)$ decreases with increasing the interaction strength. This kind of behaviour is also seen in QMC calculations of finite lattices through extrapolation [24]. The superconducting state persists to higher disorder values with increasing U in the weak to moderate coupling regime, in contrast to the strong coupling regime. We have marked the phases that would be obtained in different regions of the $x - U$ plane. There are a few things to note. The large x region must be an Anderson insulator, while the region close to the x_c line is a Bose-insulator. Naturally, within CPA, there is no way to access Anderson localization. For this reason, coupled with the speculation that we must expect crossovers instead of

phase transitions, the phase boundaries have not been marked. However, a more comprehensive approach such as statistical dynamical mean field theory should be able to complete the 'phase diagram' shown here.

2.6 Conclusions

In this chapter, we have studied the effects of site-disorder on a s-wave superconducting state as represented by an inhomogeneous attractive Hubbard model. Our theoretical approach combines DMFT with IPTSC as an impurity solver and the CPA. Detailed studies of (a) the clean system away from half-filling and (b) probability distributions of the spectral gap and order parameter have been carried out. We have computed single-particle quantities such as the diagonal and off-diagonal spectral functions in the disorder-U plane. Using these, we obtained the spectral gap, superconducting order parameter and their probability distributions for different values of disorder and interaction strength. Some of our results agree qualitatively with those of previous studies [19, 20, 22, 24]. These include the non-monotonic dependence of the spectral gap on the interaction strength, the destruction of the superconducting state with disorder and a concomitant superconductor-insulator transition. These studies [19, 20, 22, 24] were carried out on two-dimensional lattices, while our work is within DMFT. Thus, we conclude that dimensionality has little role to play in these results. We further argue that our results may be explained by utilizing particle-hole asymmetry and disorder induced probability distributions, with no necessity to invoke localization physics.

In order to probe localization physics within local approaches, one must ideally incorporate short-range correlations using techniques such as typical medium theory [29–31], typical medium-dynamical cluster approximation [33]. The extension of our results to finite temperature and general fillings would pave the way to comparison with experiments.

Bibliography

[1] Lee P A and Ramakrishnan T V 1985 Rev. Mod. Phys. **57** 287.

[2] Belitz D and Kirkpatrick T R 1994 Rev. Mod. Phys. **66** 261.

[3] Mintu Mondal *et. al* 2011 Phys. Rev. Lett. **106** 047001.

[4] Madhavi Chand *et. al* 2012 Phys. Rev. B **85** 014508.

[5] Mintu Mondal *et. al* 2013 Scientific Reports **3**, 1357 .

[6] Crane R *et. al* 2007 Phys. Rev. B **75** 184530.

[7] Benjamin Sacépé *et. al* 2010 Nature Communications **1** 140.

[8] Benjamin Sacépé *et. al* 2011 Nature Physics **7** 239-244.

[9] Micnas R, Ranninger J and Robaszkiewicz S 1990 Rev. Mod. Phys. **62** 113.

[10] Garg A, Krishnamurthy H R and Randeria M 2005 Phys. Rev. B **72** 024517.

[11] Bauer J, Hewson A C and Dupuis N 2009 Phys. Rev. B **79** 214518.

[12] Akihisa Koga and Philipp Werner 2011 Phys. Rev. A **84** 023638.

[13] Georges A, Kotliar G, Krauth W and Rozenberg M J 1996 Rev. Mod. Phys. **68** 13.

[14] Kotliar G and Vollhardt D 2004 Physics Today **57** 53-59.

[15] Vollhardt D 2010 AIP Conference Proceedings **1297**, 339.

[16] Masaru Sakaida, Kazuto Noda and Norio Kawakami 2013 J. Phys. Soc. Japan **82** 074715.

[17] Anderson P W J 1959 Phys. Chem. Solids **11** 26.

[18] Abrikosov A A and Gor'kov L P 1959 Sov. Phys. JETP **9** 220.

[19] Ghosal A, Randeria M and Trivedi N 1998 Phys. Rev. Lett. **81** 3940-3943.

[20] Ghosal A, Randeria M and Trivedi N 2001 Phys. Rev. B **65** 014501.

[21] Yonatan Dubi, Yigal Meir and Yshai Avishai 2007 Nature **449** 876.

[22] Sanjeev Kumar and Prabuddha B Chakraborty 2013 arxiv:1302.1967.

[23] Trivedi N, Scalettar R T and Randeria M 1996 Phys. Rev. B **54** R3756.

[24] Scalettar R T, Trivedi N and Huscroft C 1999 Phys. Rev. B **59** 4364.

[25] Karim Bouadim, Yen Lee Loh, Mohit Randeria and Nandini Trivedi 2011 Nature Physics **7** 884-889.

[26] Elliott R J, Krumhansl J A and Leath P L 1974 Rev. Mod. Phys. **46** 465.

[27] Janiš V and Vollhardt D 1992 Phys. Rev. B **46** 15712.

[28] Feigel'man M V, Ioffe L B, Kravtsov V E and Yuzbashyan E A 2007 Phys. Rev. Lett. **98** 027001.

[29] Dobrosavljević V, Pastor A A and Nikolić B K 2003 Europhys. Lett. **62** 76.

[30] Krzysztof Byczuk, Walter Hofstetter and Dieter Vollhardt 2005 Phys. Rev. Lett. **94**, 056404.

[31] Krzysztof Byczuk, Walter Hofstetter and Dieter Vollhardt 2005 Physica B **359-361**, 651.

[32] Potthoff M and Balzer M 2007 Phys. Rev. B **75**, 125112.

[33] Chinedu E Ekuma *et. al* 2013 arXiv:1306.5712.

Chapter 3

Interaction-disorder driven metal-superconductor transition

3.1 Introduction

In the previous chapter, we considered the effects of site-energy disorder in s-wave superconductors. The site-energies were considered to be a distributed uniformly in the energy range $[-W/2, W/2]$. In this chapter, we will consider interaction-disorder in the attractive Hubbard model. This basically means that the local attractive interactions will be considered as randomly distributed. The other model parameters such as hopping, or site-energies will be identical throughout the lattice. Such a scenario of interaction disorder in s-wave superconductors may not be far-fetched, and might be appropriate for real systems such as Tl-doped PbTe.

The semiconducting PbTe, when doped with Tl ($Pb_{1-x}Tl_xTe$), exhibits a superconducting ground state [12,13] beyond a critical concentration ($x = x_c = 0.3\%$) of Tl. The consensus regarding the origin of such doping induced superconductivity is that the Tl dopants represent spatially inhomogeneous centers of negative attractive interactions ($-U$), which nucleate Cooper pairing, and hence lead to superconductivity [14]. The variation of superconducting critical temperature (T_c) and dc resistivity (inset) of $Pb_{1-x}Tl_xTe$ as a function of x is shown in figure 3.1. It is seen that the transition temperature, T_c, increases with increasing x thus supporting the idea that Tl-dopants nucleate superconductivity.

The spatial distribution of attractive interaction centers may be mathematically represented by
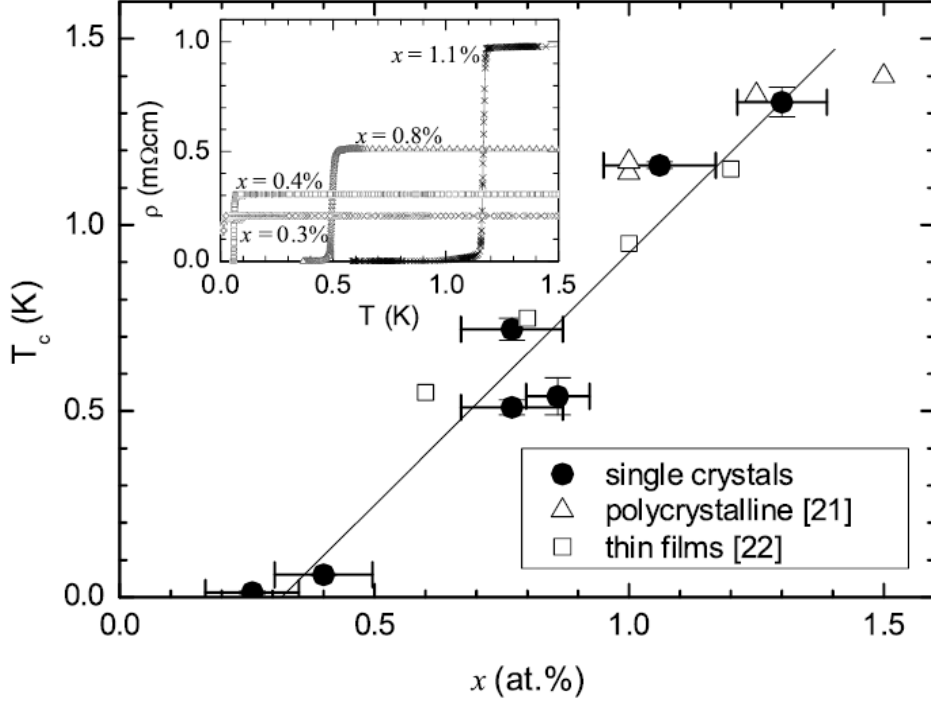
Figure 3.1: Superconducting critical temperature and dc resistivity (inset) as a function of x (From Ref. [12, 13]).

the attractive Hubbard model (AHM), with random attractive Hubbard interactions. In this chapter, we investigate such a model using the same techniques as the previous chapter. To summarise briefly just for completion, we use the framework of dynamical mean field theory (DMFT) [15–17] combined with coherent potential approximation (CPA) [18,19]. We employ two impurity solvers within DMFT: iterated perturbation theory for superconducting case (IPTSC) [21] and static mean-field theory [20]. The random interaction is taken to be distributed according to a bimodal probability distribution. While x fraction of sites have an attractive interaction, $-U$, $1-x$ fraction of sites are non-interacting. It is observed that beyond a critical $x = x_c$ the system is superconducting, but for large U values, a small value of x is sufficient to make whole system superconducting. The clean limit of the AHM has been extensively studied using Bogoliubov-de Gennes type mean field (BdGMF) theories and more recently using iterated perturbation theory with superconducting bath (IPTSC) [21], numerical renormalization group (NRG) [22] and continuous time quantum Monte Carlo (CTQMC) [23] within

DMFT. The main issue that has been focused upon is the BCS-BEC crossover for different fillings and interaction strengths.

In this chapter, we carry out a detailed study of the AHM with inhomogeneous interaction by combining CPA with DMFT and iterated perturbation theory for superconductivity(IPTSC). To distinguish between dynamical and static effects, we have also carried out BdGMF studies within CPA+DMFT. This chapter is structured as follows: In the following section, we outline the model and the formalism used. Next, we present our results for the local order parameter and spectra. We conclude in the final section.

3.2 Model and Method

We consider the single band attractive Hubbard model(AHM), which is given by the following Hamiltonian,

$$\mathcal{H} = \sum_{i\sigma} \varepsilon c_{i\sigma}^{\dagger} c_{i\sigma} - t \sum_{\langle ij\sigma \rangle} \left(c_{i\sigma}^{\dagger} c_{j\sigma} + h.c \right) - \sum_{i} |U_i| \left(n_{i\uparrow} - \frac{1}{2} \right) \left(n_{i\downarrow} - \frac{1}{2} \right) - \mu \sum_{i\sigma} c_{i\sigma}^{\dagger} c_{i\sigma} \qquad (3.1)$$

Where $c_{i\sigma}$ annihilates an electron on i^{th} lattice site with spin σ, and $n_{i\sigma} = c_{i\sigma}^{\dagger} c_{i\sigma}$, t is nearest neighbour hopping matrix, ε is onsite energy, and μ is chemical potential. The local disorder is given by random attractive Hubbard interaction, which is distributed according to the bimodal probability distribution function $P_U(U_i)$

$$P_U(U_i) = (1-x)\delta(U_i) + x\delta(U_i + U), \qquad (3.2)$$

where $1-x$ and x are fractions of lattice sites with interaction $U_i = 0$ and $U_i = -U$, respectively. To discuss how disorder affects superconductivity, we use CPA with DMFT. The impurity Green's function in Nambu formalism is given as

$$\hat{G}^i(\omega) = \begin{bmatrix} \omega^+ + \mu - \varepsilon - \Delta_{11}(\omega^+) - \Sigma_i(\omega^+) & -\Delta_{12}(\omega^+) - S_i(\omega^+) \\ -\Delta_{21}(\omega^+) - S_i(\omega^+) & \omega^+ - \mu + \varepsilon - \Delta_{22}(\omega^+) + \Sigma_i^*(-\omega^+) \end{bmatrix}^{-1} \qquad (3.3)$$

where, Δ_{11}, Δ_{12}, Δ_{21} and Δ_{22} are components of the hybridisation function matrix $\hat{\Delta}$, and Σ_i and S_i are normal and anomalous self-energies respectively. Now, by an doing arithmetic averaging over Hubbard interaction, the average local Green's function is given as

$$\hat{G}^{CPA}(\omega^+) = \int dU_i \hat{G}_i(\omega^+) P_U(U_i) \tag{3.4}$$

From equations (3.2, 3.3, and 3.4) $\hat{G}^{CPA}(\omega^+)$ is given by:,

$$\hat{G}^{CPA}(\omega^+) = (1-x)\hat{G}^0(\omega^+) + x\hat{G}^U(\omega^+) \tag{3.5}$$

where $\hat{G}^0(\omega^+)$ and $\hat{G}^U(\omega^+)$ are given by

$$\hat{G}^0(\omega) = \begin{bmatrix} \omega^+ + \mu - \varepsilon - \Delta_{11}(\omega^+) & -\Delta_{12}(\omega^+) \\ -\Delta_{21}(\omega^+) & \omega^+ - \mu + \varepsilon - \Delta_{22}(\omega^+) \end{bmatrix}^{-1} \tag{3.6}$$

$$\hat{G}^U(\omega) = \begin{bmatrix} \omega^+ + \mu - \varepsilon - \Delta_{11}(\omega^+) - \Sigma_U(\omega^+) & -\Delta_{12}(\omega^+) - S(\omega^+) \\ -\Delta_{21}(\omega^+) - S(\omega^+) & \omega^+ - \mu + \varepsilon - \Delta_{22}(\omega^+) + \Sigma^*(-\omega^+) \end{bmatrix}^{-1} \tag{3.7}$$

To calculate $\Sigma(\omega^+)$ and $S(\omega^+)$ we employ the iterated perturbation theory for superconductivity (IPTSC) [21] as an impurity solver. $\Sigma(\omega^+)$ and $S(\omega^+)$ are given by :,

$$\Sigma(\omega^+) = -U\frac{n}{2} + A\Sigma^{(2)}(\omega^+) \tag{3.8}$$

$$S(\omega^+) = -U\Phi + AS^{(2)}(\omega^+) \tag{3.9}$$

$$\Sigma^{(2)}(\omega^+) = U^2 \int_{-\infty}^{\infty} \prod_{i=1}^{3} d\varepsilon_i \frac{g_1(\varepsilon_1, \varepsilon_2, \varepsilon_3) N(\varepsilon_1, \varepsilon_2, \varepsilon_3)}{\omega^+ - \varepsilon_1 + \varepsilon_2 - \varepsilon_3} \tag{3.10}$$

$$S^{(2)}(\omega^+) = U^2 \int_{-\infty}^{\infty} \prod_{i=1}^{3} d\varepsilon_i \frac{g_2(\varepsilon_1, \varepsilon_2, \varepsilon_3) N(\varepsilon_1, \varepsilon_2, \varepsilon_3)}{\omega^+ - \varepsilon_1 + \varepsilon_2 - \varepsilon_3} \tag{3.11}$$

$$\mathscr{G}^U(\omega) = \begin{bmatrix} \omega^+ + \mu - \varepsilon - \Delta_{11}(\omega^+) + U\frac{n}{2} & -\Delta_{12}(\omega^+) + U\Phi \\ -\Delta_{21}(\omega^+) + U\Phi & \omega^+ - \mu + \varepsilon - \Delta_{22}(\omega^+) - U\frac{n}{2} \end{bmatrix}^{-1} \tag{3.12}$$

$$-\mathrm{Im}\frac{\hat{\mathscr{G}}^{\mathrm{U}}(\omega^+)}{\pi} = \left[\begin{array}{cc} \tilde{\rho}_{11}(\omega) & \tilde{\rho}_{12}(\omega) \\ \tilde{\rho}_{21}(\omega) & \tilde{\rho}_{22}(\omega) \end{array}\right] \tag{3.13}$$

$$N(\varepsilon_1,\varepsilon_2,\varepsilon_3) = f(\varepsilon_1)f(-\varepsilon_2)f(\varepsilon_3) + f(-\varepsilon_1)f(\varepsilon_2)f(-\varepsilon_3) \tag{3.14}$$

$$g_1(\varepsilon_1,\varepsilon_2,\varepsilon_3) = \tilde{\rho}_{11}(\varepsilon_1)\tilde{\rho}_{22}(\varepsilon_2)\tilde{\rho}_{22}(\varepsilon_3) - \tilde{\rho}_{12}(\varepsilon_1)\tilde{\rho}_{22}(\varepsilon_2)\tilde{\rho}_{12}(\varepsilon_3) \tag{3.15}$$

$$g_2(\varepsilon_1,\varepsilon_2,\varepsilon_3) = \tilde{\rho}_{12}(\varepsilon_1)\tilde{\rho}_{12}(\varepsilon_2)\tilde{\rho}_{12}(\varepsilon_3) - \tilde{\rho}_{11}(\varepsilon_1)\tilde{\rho}_{12}(\varepsilon_2)\tilde{\rho}_{22}(\varepsilon_3) \tag{3.16}$$

$$A = \frac{\frac{n}{2}(1-\frac{n}{2})-\Phi^2}{\frac{n_0}{2}(1-\frac{n_0}{2})-\Phi_0^2} \tag{3.17}$$

where Φ, Φ_0, n and n_0 are given by :,

$$\Phi = \int_{-\infty}^{\infty} d\omega \frac{-\mathrm{Im}(\mathrm{G}_{12}^{\mathrm{U}}(\omega^+))}{\pi} f(\omega) \tag{3.18}$$

$$\Phi_0 = \int_{-\infty}^{\infty} d\omega \tilde{\rho}_{12}(\omega)f(\omega) \tag{3.19}$$

$$n = 2\int_{-\infty}^{\infty} d\omega \frac{-\mathrm{Im}(\mathrm{G}_{11}^{\mathrm{U}}(\omega^+))}{\pi} f(\omega) \tag{3.20}$$

$$n_0 = 2\int_{-\infty}^{\infty} d\omega \tilde{\rho}_{11}(\omega)f(\omega) \tag{3.21}$$

The CPA Green's function in term of average self-energy is given by

$$\hat{G}^{CPA}(\omega^+) = \left[\begin{array}{cc} \omega^+ - \varepsilon + \mu - \Delta_{11}(\omega^+) - \Sigma_{11}^{CPA}(\omega^+) & -\Delta_{12}(\omega^+) - \Sigma_{12}^{CPA}(\omega^+) \\ -\Delta_{21}(\omega^+) - \Sigma_{21}^{CPA}(\omega^+) & \omega^+ + \varepsilon - \mu - \Delta_{22}(\omega^+) - \Sigma_{22}^{CPA}(\omega^+) \end{array}\right]^{-1} \tag{3.22}$$

The lattice Green's function is given by :,

$$\hat{G}(\vec{k},\omega^+) = \left[\begin{array}{cc} \omega^+ - \varepsilon + \mu - \varepsilon(\vec{k}) - \Sigma_{11}^{CPA}(\omega^+) & -\Sigma_{12}^{CPA}(\omega^+) \\ -\Sigma_{21}^{CPA}(\omega^+) & \omega^+ + \varepsilon - \mu + \varepsilon(\vec{k}) - \Sigma_{22}^{CPA}(\omega^+) \end{array}\right]^{-1} \tag{3.23}$$

Finally, the CPA self-consistency is achieved by equating the local Green's function to average impurity Green's function :,

$$\frac{1}{N_s}\sum_{\vec{k}} \hat{G}(\vec{k},\omega^+) = \hat{G}^{CPA}(\omega^+) \tag{3.24}$$

Where, N_s is the number of lattice sites.

3.3 Numerical Algorithm

In practice, we follow the steps outlined below to obtain the converged order parameter and spectra.

1. Guess a hybridization matrix $\hat{\Delta}(\omega)$ for interacting and non-interacting site and n, Φ for interacting sites. In practice, we choose either a previously converged solution or the non-interacting $\hat{\Delta}(\omega)$ with $n = 1$ and $\Phi = 1/2$.

2. Given a hybridization, occupancy and order parameter, use equation (3.12) to calculate the host Green's function matrix, $\mathscr{G}^U(\omega)$.

3. From equations (3.21 and 3.19), calculate pseudo-occupancy and pseudo-order parameter, n_0 and Φ_0.

4. Now, by using equations (3.8, 3.9, 3.10, 3.11, and 3.17) calculate the regular and anomalous self-energies, $\Sigma(\omega)$ and, $S(\omega)$.

5. Then, by using equations (3.6, 3.7, 3.8, and 3.9), calculate impurity Green's function $\hat{G}^0(\omega)$, $\hat{G}^U(\omega)$ n and, Φ .

6. The disorder-averaged Green's function, $\hat{G}^{CPA}(\omega)$ is obtained using equation (3.5).

7. We consider the AHM on Bethe lattice of infinite connectivity at half filling, which is achieved by setting $\mu = 0, \varepsilon = 0$. For Bethe lattice the self-consistency condition is simply given by :,

$$\hat{\Delta}(\omega) = \frac{t^2 \sigma_z \hat{G}^{CPA}(\omega) \sigma_z}{4} \tag{3.25}$$

where σ_z is z component of Pauli's matrix. Using equation (3.25), a new hybridization matrix $\hat{\Delta}$ is obtained.

8. If the hybridization matrix $\hat{\Delta}(\omega)$ from step 7 and n, Φ from step 5 are equal (within a desired numerical tolerance) to the guess hybridization matrix $\hat{\Delta}(\omega)$, n and Φ from step 1, then the iterations may be stopped, else the iterations continue until the desired convergence is achieved.
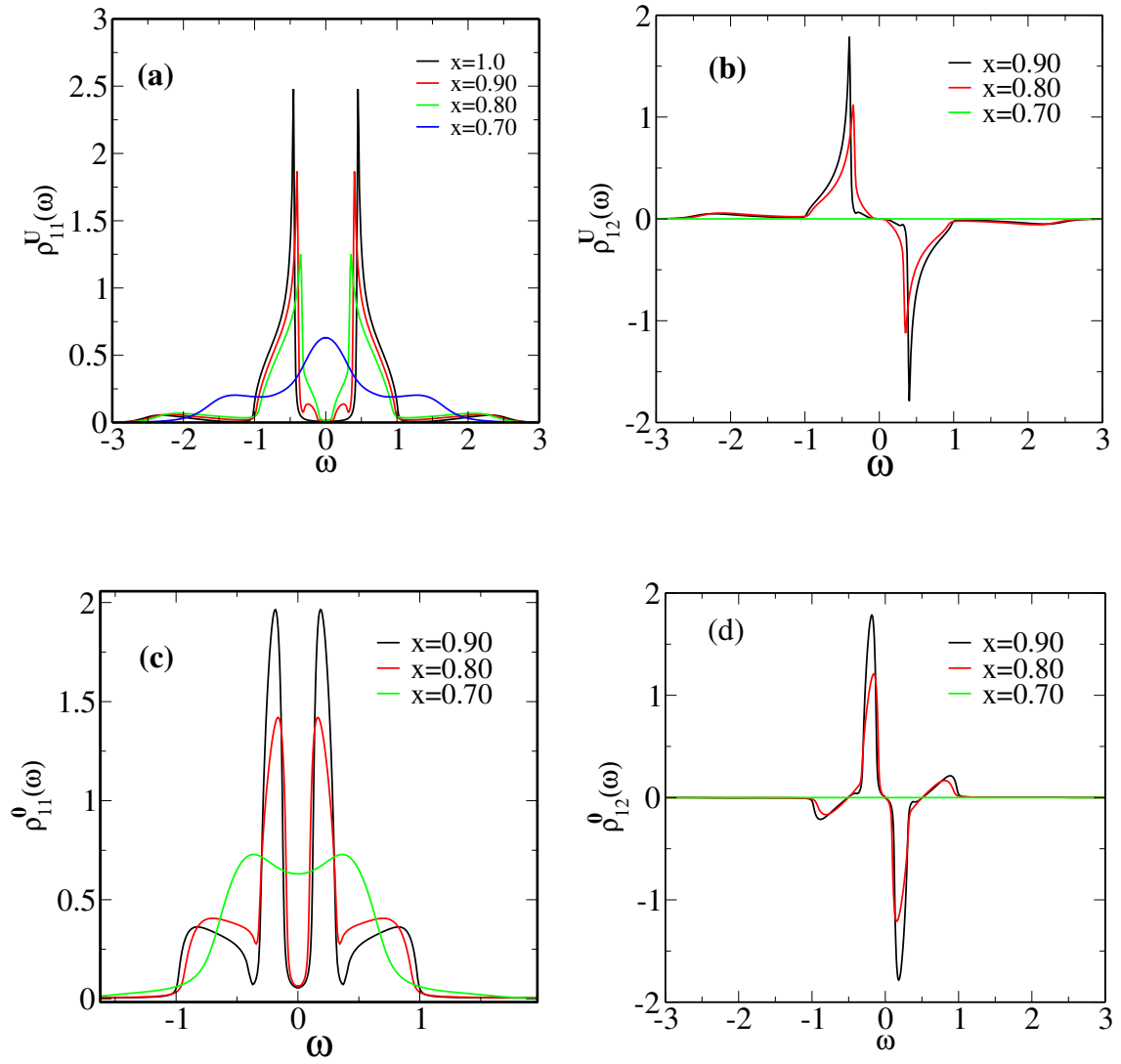
Figure 3.2: Diagonal(a,b) and off diagonal(c,d) spectral function as a function of frequency for inter-acting and non-interacting site respectively at U=1.5.

3.4 Results and Discussion

In this chapter, we have considered $1 - x$ fraction of the sites to be non-interacting ($U = 0$), and x fraction to be interacting ($U \neq 0$). The unit of energy is the hopping integral $t = 1$. We have done all the calculations at half filling ($\langle n \rangle = 1$), which is fixed by taking $\mu = \varepsilon = 0$.

3.4.1 Spectral functions

In figure 3.2, the 11 and 12 components of local spectral functions as a function of frequency are shown for different values of x at $U = 1.5$. The panel (a) and (b) represent the 11 and 12 components of spectral function of interacting site respectively. $\rho_{11}^U(\omega)$, $\rho_{12}^U(\omega)$, $\rho_{11}^0(\omega)$, and $\rho_{12}^0(\omega)$ represent the 11 and 12 components of local spectral function of the interacting and non-interacting sites respectively. For a $U = 1.5$, we find that, beyond a critical value of $x \sim 0.70$ the $\rho_{11}^U(\omega)$ becomes gapped, and the gap increases with increasing x. The spectral function has coherence peaks at the gap edges, and the weight of the coherence peak increases with increasing x. Concomitantly, beyond $x \sim 0.70$, the off-diagonal spectrum, $\rho_{12}^U(\omega)$ develops finite spectral weight, which increases with increasing x. This also implies that the local superconducting order parameter, Φ, given by integration of $\rho_{12}^U(\omega)$ upto the Fermi level, increases with increasing x. Thus we conclude that the spectral gap of figure 3.2(a) is superconducting in nature. We find that the non-interacting sites also develop superconductivity. This is seen from the evolution of the local spectral functions corresponding to the non-interacting sites, which are shown in the two lower panels of figure 3.2. This is natural because the host in which the interacting and non-interacting sites are embedded, characterized by $\Delta(\omega)$, becomes superconducting.

In figure 3.3 the 11 component of disorder averaged spectral function is shown for various values of x computed with $U = 1.5, 1.6, 1.7$ and, 1.8. It is seen all the spectra are gapped at $x = 1.0$. With decreasing x, the gap shrinks, and finally a superconductor to metal transition occurs at a critical x_c. The nature of this transition and the dependence of x_c on U will be discussed next.

3.4.2 Metal-superconductor transition

The results in the previous sections suggest the following scenario: For $x = 0$, there are no sites with $-U$, and the system is a metal. With increasing x, the system develops superconductivity beyond a
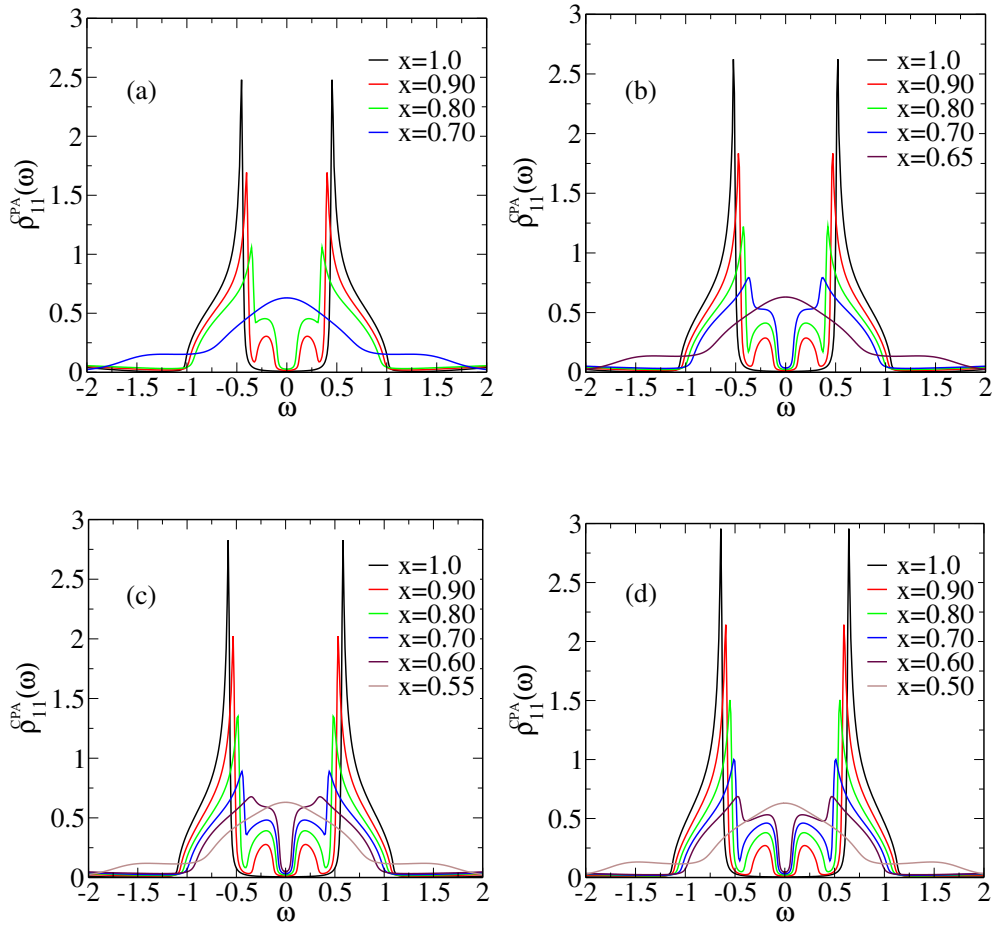
Figure 3.3: Diagonal component of CPA spectral function as a function of frequency for (a) U=1.5 (b) U=1.6 (c) U=1.7 (d) U=1.8.
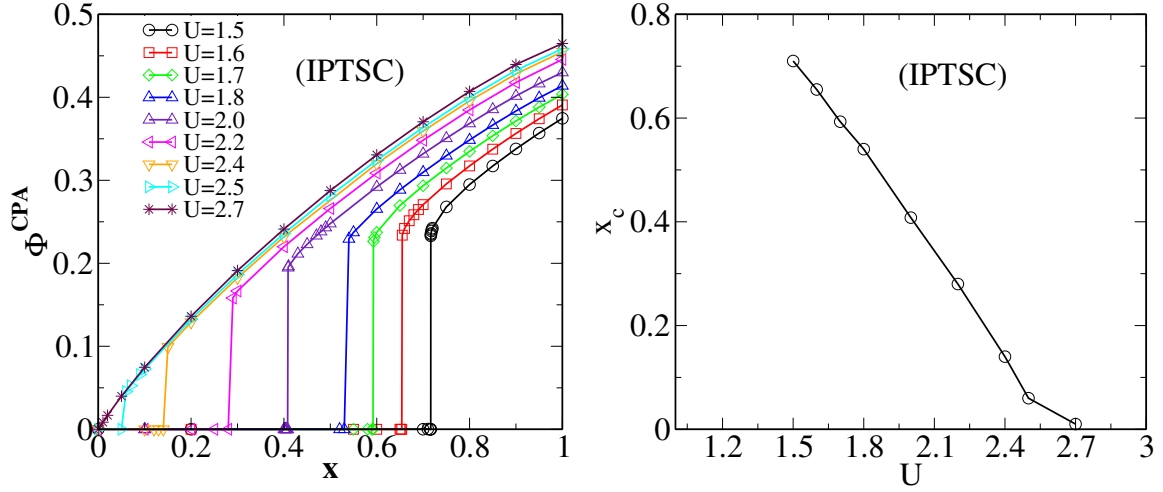
Figure 3.4: Left panel: Disorder averaged superconducting order (Φ^{CPA}) as a function of x for different values of U. Right Panel : The critical fraction of interacting sites, x_c, *vs* U.

critical x_c. The disorder averaged superconducting order parameter (Φ^{CPA}), calculated by using the expression,

$$\Phi^{CPA} = \int_{-\infty}^{\infty} d\omega \frac{-\text{Im}(G_{12}^{\text{CPA}}(\omega^+))f(\omega)}{\pi}, \qquad (3.26)$$

is shown in left panel of figure 3.4 as a function of x for different values of U. For all $U \lesssim 2.7$, a finite x_c is needed before the superconducting order develops. The transition from metal to superconductor is seen to be first order. The critical x_c decreases sharply with increasing U as seen in the right panel. For all $U \geqslant 2.7$, the transition becomes continuous and the critical x_c needed to generate superconductivity is practically zero. This indicates that the interaction stabilises the superconducting phase in presence of disorder.

3.4.3 Comparison of IPTSC and BdGMF results

We would like to understand the precise effect of incorporating dynamics beyond static mean field solutions. Hence we compare a few representative results from IPTSC with those from BdGMF. figure 3.5 depicts this comparison. The Φ^{CPA} computed with BdGMF and IPTSC are shown in panels (a) and (b) respectively. As seen, the BdGMF Φ^{CPA} increases continuously with increasing x, while
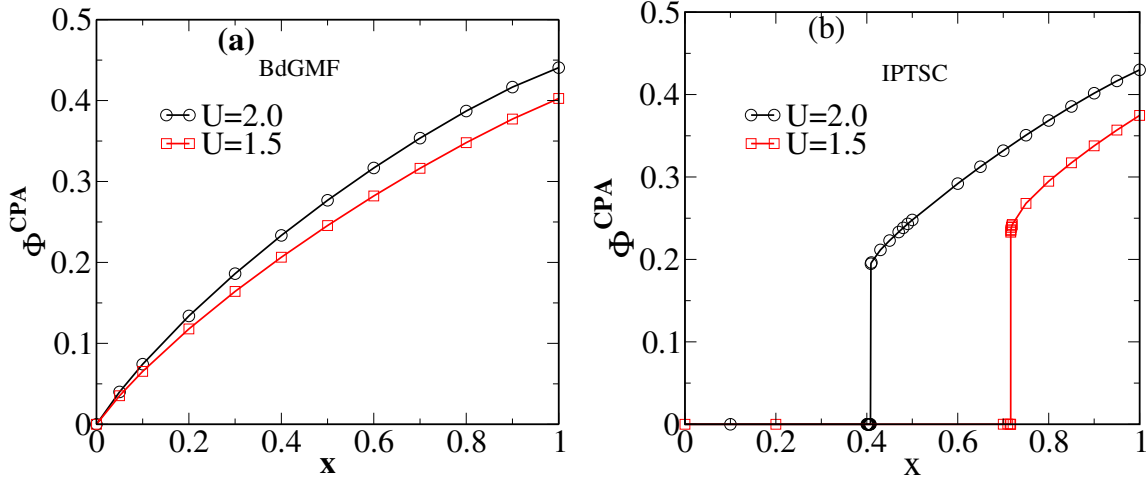
Figure 3.5: The disorder-averaged superconducting order parameter, Φ^{CPA}, as a function of disorder, x computed within BdGMF (left panel) and IPTSC (right panel).

the DMFT calculation using IPTSC as the solver shows a first order transition. Thus,incorporating dynamics changes the qualitative nature of the metal-superconductor transition.

3.5 Conclusions

In this chapter, a disordered attractive Hubbard model with spatially random interaction sites is investigated by combining DMFT, CPA and IPTSC as an impurity solver at half filling. We have computed local quantities such as diagonal and off diagonal spectral function for different values of U and x. By using local diagonal and off diagonal spectral functions, we have computed spectral gap and superconducting order parameter. We find a doping (disorder) induced metal to superconductor transition. The transition is first order for low interaction strengths, but becomes continuous for $U > U_c$. The critical disorder needed to achieve superconductivity becomes zero beyond $U > U_c$. To understand the effects of including dynamical fluctuations beyond static mean-field, we have calculated the superconducting order parameter in IPTSC and BdGMF frameworks. In parallel to the IPTSC scenario described above, the BdGMF approach shows a metal to superconductor transition, however the transition is always continuous and $x_c = 0$ for all U.

3.6 Comparison between site energy disorder and binary disorder in interaction results

In chapter 2, we had considered site-energy disorder. We had seen that the superconducting order parameter (Φ^{CPA}) in both IPTSC and BdGMF approaches are nearly same, and the system shows a continuous superconductor to insulator transition. In this chapter, we observe that the dependence of Φ^{CPA} on x and U as computed with the IPTSC and BdGMF approaches are very different. With site-disorder, Φ^{CPA} invariably decreased with increasing interaction for a given value of x and in large interaction limit, the superconducting state becomes less robust. With interaction-disorder, Φ^{CPA} increases with increasing U for a given value of x, and superconducting state becomes more robust in the large interaction limit. Dynamical fluctuations change the static mean field results only marginally in the presence of site-disorder; while we see that inclusion of dynamics beyond static mean-field can change the character of the metal-superconductor transition qualitatively when the randomness is in the interaction strength.

Bibliography

[1] Lee P A and Ramakrishnan T V 1985 Rev. Mod. Phys. **57** 287.

[2] Belitz D and Kirkpatrick T R 1994 Rev. Mod. Phys. **66** 261.

[3] Phase Separation in Cuprate Superconductors, edited by E Sigmund and K A Muller (Springer, Heidelberg, 1994).

[4] Howald C, Fournier P, and Kapitulnik A, 2001 Phys. Rev. B **64** 100504 .

[5] Pan S H *et. al* 2001 Nature(London) **413** 282 .

[6] Hanaguri T *et. al* 2004 Nature (London) **430**, 1001 .

[7] Vershinin M *et. al* 2004 Science **303** 1995 .

[8] McElroy K *et. al* 2005 Science **309** 1048 .

[9] Rourke P M C *et. al* 2005 Phys. Rev. Lett. **94** 107005 .

[10] Gomes K K *et. al* 2007 Nature (London) **447** 569 .

[11] Gomes K K *et. al* 2007 Physica C **460-462** 212 .

[12] Matsushita Y 2005 *et. al* Phys. Rev. Lett. **94** 157002.

[13] Matsushita Y *et. al* 2006 Phys. Rev. B **74** 134512 .

[14] Micnas R, Ranninger J and Robaszkiewicz S 1990 Rev. Mod. Phys. **62** 113.

[15] Georges A, Kotliar G, Krauth W and Rozenberg M J 1996 Rev. Mod. Phys. **68** 13.

[16] Kotliar G and Vollhardt D 2005 Physics Today .

[17] Vollhardt D AIP Conference Proceedings 2010 **1297** 339.

[18] Elliott R J, Krumhansl J A and Leath P L 1974 Rev. Mod. Phys. **46**, 465.

[19] Janis V and Vollhardt D Phys. Rev. B 1992 **46** 15712.

[20] Vijay B Shenoy 2008 Phys. Rev. B **78** 134503.

[21] Garg A, Krishnamurthy H R and Randeria M 2005 Phys. Rev. B **72** 024517.

[22] Bauer J, Hewson A C, and Dupuis N 2009 Phys. Rev. B **79** 214518.

[23] Akihisa Koga and Philipp Werner 2011 Phys. Rev. A **84** 023638.

Chapter 4

Proximity of superconductor to normal metal

4.1 Introduction

The physical proximity of two or more distinct phases of matter can generate exotic phenomena at the interface. Spectacular examples of such phenomena include formation of a depletion layer at p-n junctions, giant magnetoresistance effect in alternating ferromagnetic and non-magnetic metallic heterostructures, formation of a two-dimensional electron gas at the interface of a band insulator and a Mott insulator. Similarly, when a superconductor is brought into contact with a normal metal or a ferromagnet, then many interesting phenomena take place at the interfaces such as Andreev reflection [1], induction of superconducting correlations in normal metal, triplet pairing at the interface of superconductor and ferromagnet etc. These phenomena are collectively known as proximity effects.

The proximity of the superconductor to normal metal is, theoretically, a well studied problem [2–4], albeit with static mean field theories. The consensus from these studies is that the superconducting transition temperature decreases with increasing the thickness of the normal metal layer. There are many experimental realizations of the superconductor-normal metal(SN) interface, such as Nb/Au [5, 6] and $NbSe_2$/Au [7]. Similarly, proximity effects in a superconductor-ferromagnet(SF) interface have been realized in Nb/Fe [8–10], Nb/Gd [11, 12], V/Fe [13–15], $V/V_{1-x}Fe_x$ [16], Pb/Fe [17], Co/Al [18], and $YBa_2Cu_3O_{7-\delta}/La_{0.7}Co_{0.3}MnO_3$ [19] etc. At an SN or an SF interface, it is observed that the superconductivity is induced in the metallic/ferromagnetic (M/FM) layer because of leakage of Cooper pairs from superconductor to M/FM. The superconducting transition temperature decreases

with increasing the thickness of the non-SC second layer. The magnetic moments in ferromagnet break Cooper pairs inside the ferromagnet because of breaking of time reversal symmetry and hence the superconducting critical temperature decreases as function of thickness of ferromagnetic layer faster than SN layer.

In a recent theoretical study, an SN interface has been represented by a bilayer attractive Hubbard model on a square lattice of finite size. The model has been solved using Quantum Monte Carlo (QMC) as well as Bogoliubov-de Gennes mean field approximation [20]. The superconducting layer is considered interacting ($U < 0$), while the other layer is taken to be non-interacting ($U = 0$). The layers are connected by an inter-planar hopping ($t_\perp$). It was found that the pair-correlation function in the interacting plane decreases with increasing $t_\perp$ and beyond a critical value of $t_\perp = t_{c\perp}$, it completely vanishes. The non-interacting plane shows non-monotonic behaviour: the pair-correlation increases with increasing $t_\perp$, reaches a maximum, and then decreases with further increasing $t_\perp$, and finally vanishes beyond $t_{c\perp}$. For $t_\perp > t_{c\perp}$, both the layers become non-superconducting.

In this chapter, we have studied the bilayer attractive Hubbard model (AHM) by combining DMFT [21–23] and IPTSC [24–26] as an impurity solver. Although the target system is the same as that of Ref. [20], our method allows us to study the thermodynamic limit, thus avoiding any finite-size effects. This chapter is structured as follows: In the following section, we outline the model and the formalism used. Next, we present our results for the spectra and order parameter. We conclude in the final section.

4.2 Model and Method

We consider a single band bilayer attractive Hubbard model (AHM), which may be represented by the following Hamiltonian:

$$\mathscr{H} = \sum_{i\sigma,l=1}^{l=2} \varepsilon_l c_{il\sigma}^\dagger c_{il\sigma} - \sum_{<ij\sigma>,l=1}^{l=2} t_l [c_{il\sigma}^\dagger c_{jl\sigma} + h.c] - \sum_{i,l=1}^{l=2} |U_l| (n_{il\uparrow} - \frac{1}{2})(n_{il\downarrow} - \frac{1}{2}) -$$
$$\sum_{i\sigma,l=1}^{l=2} \mu_l c_{il\sigma}^\dagger c_{il\sigma} - t_\perp \sum_{i\sigma} [c_{i1\sigma}^\dagger c_{i2\sigma} + h.c] \qquad (4.1)$$

where $c_{il\sigma}$ annihilates an electron with spin σ on the ith lattice site in the lth plane. The local occupancy is determined by the operator, $n_{il\sigma} = c_{il\sigma}^{\dagger} c_{il\sigma}$. The indices i, j run over the lattice sites in each plane and l is a plane index. $t_{\perp}$ is inter planer hopping and t_l is intra-planar hopping in the l_{th} plane; ε_l is the site energy of l_{th} plane.

To take superconductivity into account, we use four components Nambu spinor, which is defined as

$$\Psi_k = \begin{bmatrix} c_{k1\uparrow} \\ c_{-k1\downarrow}^{\dagger} \\ c_{k2\uparrow} \\ c_{-k2\downarrow}^{\dagger} \end{bmatrix} \tag{4.2}$$

The matrix Green's function is given by

$$\hat{G}(\vec{k}, \tau) = - < T_{\tau} \Psi \ (\vec{k}, \tau) \Psi^{\dagger}(\vec{k}, 0) > \tag{4.3}$$

where 1 and 2 label the planes and $\vec{k}$ is momentum quantum number. The Green's function in absence of interaction ($U_1 = U_2 = 0$) is given by

$$\hat{G}_0(\vec{k}, \omega) = \begin{bmatrix} \omega^+ - \bar{\varepsilon}_1(\vec{k}) & 0 & t_{\perp} & 0 \\ 0 & \omega^+ + \bar{\varepsilon}_1(\vec{k}) & 0 & -t_{\perp} \\ t_{\perp} & 0 & \omega^+ - \bar{\varepsilon}_2(\vec{k}) & 0 \\ 0 & -t_{\perp} & 0 & \omega^+ + \bar{\varepsilon}_2(\vec{k}) \end{bmatrix}^{-1} \tag{4.4}$$

where $\bar{\varepsilon}_l(\vec{k}) = \varepsilon_l(\vec{k}) - \mu_l + \varepsilon_l$ and $\varepsilon_l(\vec{k})$ is the dispersion relation for the lth plane. Then, the interacting Green's function is obtained by using the Dyson's equation

$$\hat{G}^{-1}(\vec{k}, \omega) = \hat{G}_0^{-1}(\vec{k}, \omega) - \hat{\Sigma}(\omega) \tag{4.5}$$

where $\hat{\Sigma}(\omega)$ is self-energy matrix, and is given by

$$\hat{\Sigma}(\omega) = \begin{bmatrix} \Sigma_1(\omega) & S_1(\omega) & 0 & 0 \\ S_1(\omega) & -\Sigma_1^*(-\omega) & 0 & 0 \\ 0 & 0 & \Sigma_2(\omega) & S_2(\omega) \\ 0 & 0 & S_2(\omega) & -\Sigma_2^*(-\omega) \end{bmatrix} \tag{4.6}$$

where $\Sigma_1(\omega)$, $S_1(\omega)$, $\Sigma_2(\omega)$ and $S_2(\omega)$ are the normal and anomalous self-energies of planes 1 and 2 respectively. In order to calculate the local self-energies, we use the technique of iterated perturbation theory for superconductivity (IPTSC) [24] as an impurity solver. In the IPTSC method, based on second order perturbation theory, the self-energies are given by the following ansatz:

$$\Sigma_1(\omega) = -U\frac{n_1}{2} + A_1\Sigma_1^{(2)}(\omega) \tag{4.7}$$

$$S_1(\omega) = -U\Phi_1 + A_1 S_1^{(2)}(\omega) \tag{4.8}$$

$$\Sigma_2(\omega) = -U\frac{n_2}{2} + A_2\Sigma_2^{(2)}(\omega) \tag{4.9}$$

$$S_2(\omega) = -U\Phi_2 + A_2 S_2^{(2)}(\omega) \tag{4.10}$$

where the local filling n_1, n_2 and order parameter Φ_1, Φ_2 are given by

$$n_1 = -\frac{2}{\pi}\int_{-\infty}^{\infty} d\omega\, \text{Im}(G_{11}(\omega^+))f(\omega) \tag{4.11}$$

$$\Phi_1 = \int_{-\infty}^{\infty} d\omega\, \frac{-\text{Im}(G_{12}(\omega))}{\pi}f(\omega) \tag{4.12}$$

$$n_2 = -\frac{2}{\pi}\int_{-\infty}^{\infty} d\omega\, \text{Im}(G_{33}(\omega))f(\omega) \tag{4.13}$$

$$\Phi_2 = \int_{-\infty}^{\infty} d\omega\, \frac{-\text{Im}(G_{34}(\omega))}{\pi}f(\omega) \tag{4.14}$$

and $f(\omega) = \theta(-\omega)$ is the Fermi-Dirac distribution function at zero temperature. In the ansatz above,

(equations (4.4 and 4.5)), the second order self-energies are given by

$$
\begin{aligned}
\Sigma_1^{(2)}(\omega) &= U^2 \int_{-\infty}^{\infty} \prod_{j=1}^{3} d\omega_j \frac{g_{11}(\omega_1, \omega_2, \omega_3) N(\omega_1, \omega_2, \omega_3)}{\omega^+ - \omega_1 + \omega_2 - \omega_3} \\[2mm]
S_1^{(2)}(\omega) &= U^2 \int_{-\infty}^{\infty} \prod_{j=1}^{3} d\omega_j \frac{g_{21}(\omega_1, \omega_2, \omega_3) N(\omega_1, \omega_2, \omega_3)}{\omega^+ - \omega_1 + \omega_2 - \omega_3} \\[2mm]
\Sigma_2^{(2)}(\omega) &= U^2 \int_{-\infty}^{\infty} \prod_{j=1}^{3} d\omega_j \frac{g_{12}(\omega_1, \omega_2, \omega_3) N(\omega_1, \omega_2, \omega_3)}{\omega^+ - \omega_1 + \omega_2 - \omega_3} \\[2mm]
&\text{and} \\[2mm]
S_2^{(2)}(\omega) &= U^2 \int_{-\infty}^{\infty} \prod_{j=1}^{3} d\omega_j \frac{g_{22}(\omega_1, \omega_2, \omega_3) N(\omega_1, \omega_2, \omega_3)}{\omega^+ - \omega_1 + \omega_2 - \omega_3} \quad (4.15)
\end{aligned}
$$

where

$$
\begin{aligned}
N(\omega_1, \omega_2, \omega_3) &= f(\omega_1) f(-\omega_2) f(\omega_3) + f(-\omega_1) f(\omega_2) f(-\omega_3) \\[2mm]
g_{11}(\omega_1, \omega_2, \omega_3) &= \tilde{\rho}_{11}(\omega_1) \tilde{\rho}_{22}(\omega_2) \tilde{\rho}_{22}(\omega_3) - \tilde{\rho}_{12}(\omega_1) \tilde{\rho}_{22}(\omega_2) \tilde{\rho}_{12}(\omega_3) \\[2mm]
g_{21}(\omega_1, \omega_2, \omega_3) &= \tilde{\rho}_{12}(\omega_1) \tilde{\rho}_{12}(\omega_2) \tilde{\rho}_{12}(\omega_3) - \tilde{\rho}_{11}(\omega_1) \tilde{\rho}_{12}(\omega_2) \tilde{\rho}_{22}(\omega_3) \\[2mm]
g_{12}(\omega_1, \omega_2, \omega_3) &= \tilde{\rho}_{33}(\omega_1) \tilde{\rho}_{44}(\omega_2) \tilde{\rho}_{44}(\omega_3) - \tilde{\rho}_{34}(\omega_1) \tilde{\rho}_{44}(\omega_2) \tilde{\rho}_{34}(\omega_3) \\[2mm]
g_{22}(\omega_1, \omega_2, \omega_3) &= \tilde{\rho}_{34}(\omega_1) \tilde{\rho}_{34}(\omega_2) \tilde{\rho}_{34}(\omega_3) - \tilde{\rho}_{33}(\omega_1) \tilde{\rho}_{34}(\omega_2) \tilde{\rho}_{44}(\omega_3) \quad (4.16)
\end{aligned}
$$

and the spectral functions $\tilde{\rho}_{\alpha\beta}^i$, $\alpha, \beta = 1, 4$ are given by the imaginary part of the 'Hartree-corrected' host Green's function, namely $\hat{\tilde{\rho}}(\omega) = -\text{Im}\hat{\mathscr{G}}(\omega)/\pi$. The latter is given by

$$
\mathscr{G}(\vec{k}, \omega) =
\begin{bmatrix}
\omega^+ - \bar{\varepsilon}_1(\vec{k}) + U\frac{n_1}{2} & U\Phi_1 & t_\perp & 0 \\[2mm]
U\Phi_1 & \omega^+ + \bar{\varepsilon}_1(\vec{k}) - U\frac{n_1}{2} & 0 & -t_\perp \\[2mm]
t_\perp & 0 & \omega^+ - \bar{\varepsilon}_2(\vec{k}) + U\frac{n_2}{2} & U\Phi_2 \\[2mm]
0 & -t_\perp & U\Phi_2 & \omega^+ + \bar{\varepsilon}_2(\vec{k}) - U\frac{n_2}{2}
\end{bmatrix}^{-1}
\quad (4.17)
$$

$$\mathscr{G}(\omega) = \sum_{\vec{k}} \mathscr{G}(\vec{k}, \omega)$$

$$\hat{G}(\omega) = \sum_{\vec{k}} \hat{G}(\vec{k}, \omega) \tag{4.18}$$

Finally the coefficient A_l, which is determined by the high frequency limit, in the IPTSC ansatz equations (4.7, 4.8, 4.9, and 4.10), is given by

$$A_l = \frac{\frac{n_l}{2}(1 - \frac{n_l}{2}) - \Phi_l^2}{\frac{n_{0l}}{2}(1 - \frac{n_{0l}}{2}) - \Phi_{0l}^2} \tag{4.19}$$

where the pseudo order-parameter Φ_{0l} and the pseudo occupancy n_{0l}, are given by

$$
\begin{aligned}
n_{01} =&\ 2 \int_{-\infty}^{\infty} d\omega \tilde{\rho}_{11}(\omega) f(\omega) \\
\Phi_{01} =&\ \int_{-\infty}^{\infty} d\omega \tilde{\rho}_{12}(\omega) f(\omega) \\
n_{02} =&\ 2 \int_{-\infty}^{\infty} d\omega \tilde{\rho}_{33}(\omega) f(\omega) \\
\text{and}\quad \Phi_{02} =&\ \int_{-\infty}^{\infty} d\omega \tilde{\rho}_{34}(\omega) f(\omega).
\end{aligned}
\tag{4.20}
$$

4.3 Numerical Algorithm

The algorithm to solve above equations is given below

1. Guess $\hat{\Sigma}$ and calculate $\hat{G}$ by using equations 4.4 and 4.5 .

2. Then by using equations 4.11, 4.12, 4.13, 4.14 and 4.17 calculate effective medium propagator $\mathscr{G}(\omega)$.

3. By using effective medium propagator calculate the new self-energy matrix.

4. If initial and final self-energy matrix have converged within a desired accuracy, then stop, else feedback this new self-energy to step 1.

4.4 Results and discussion

In this chapter, we have considered plane-1 to be interacting $(U_1 \neq 0)$ and plane-2 to be non-interacting $(U_2 = 0)$. Both planes are at half filling which is fixed by taking $\mu_1 = \mu_2 = \varepsilon_1 = \varepsilon_2 = 0.0$. We have taken $t_1 = t_2 = 1$ as an energy unit, and $U = 2.0$. Both layers are Bethe lattices of infinite connectivity.

4.4.1 Spectral functions

To understand the proximity effect, we have analyzed the spectral functions of both interacting $(U \neq 0)$ and non-interacting $(U = 0)$ planes for different values of $t_\perp$. In figure 4.1, the diagonal component
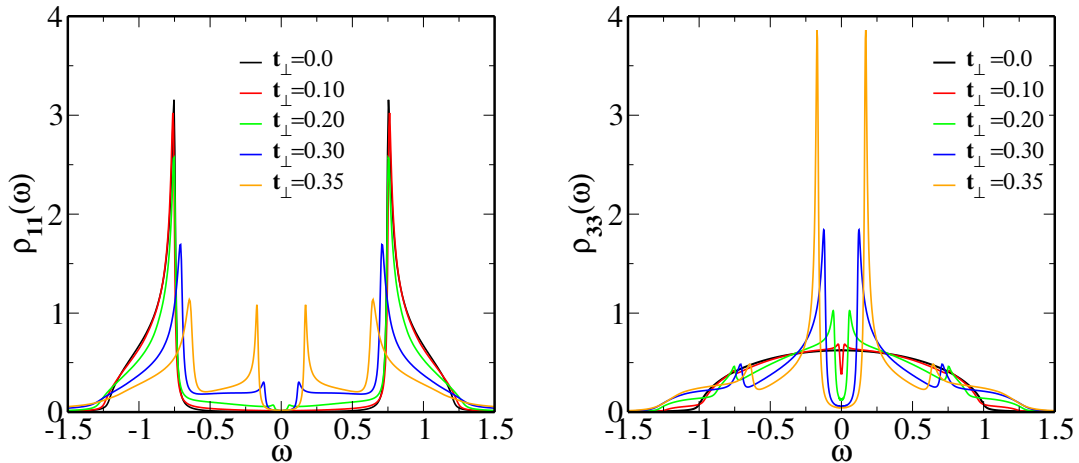

Figure 4.1: Left panel: Correlated layer; Right panel: non-interacting layer.

of the spectral function as function of ω is shown for different values of inter-planar hopping $(t_\perp)$. The left panel represents the spectral function of interacting plane while right panel represents the spectral function of the non-interacting plane. In left panel, there is a sharp coherence peak at the gap edge of spectral function at $t_\perp = 0.0$, which characteristic of s-wave superconductivity. The spectral weight of the coherence peak decreases with increasing $t_\perp$, indicating that superconducting order is melting in interacting plane because of proximity to non-interacting plane. In the right panel, at $t_\perp = 0.0$, spectral function is semi-elliptic because it is basically the non-interacting density of states of an infinite-dimensional Bethe lattice. With increasing $t_\perp$, the non-interacting spectral function becomes gapped.
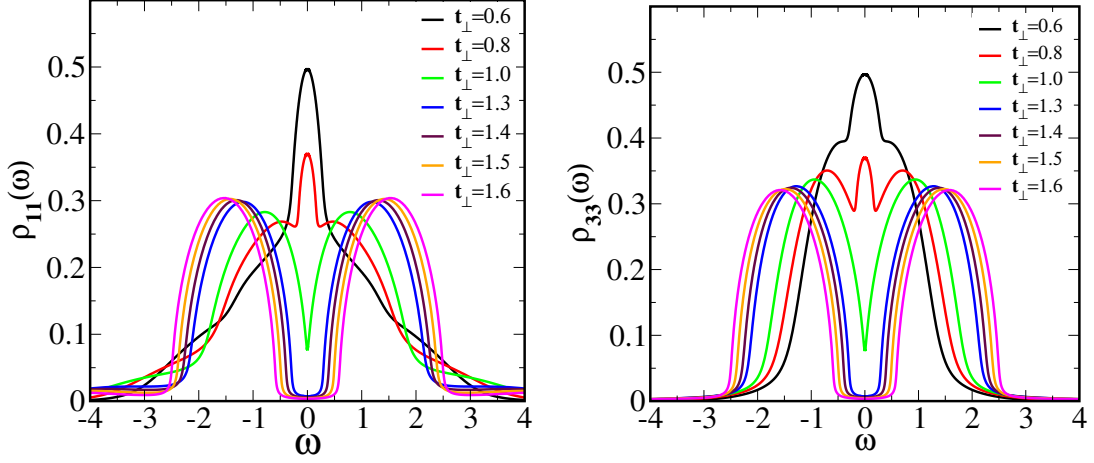
Figure 4.2: Left panel: Correlated layer; Right panel: non-interacting layer.

As will be discussed later, this gap is due to induction of superconductivity in the non-interacting layer caused by the proximity to the SC layer. At $t_\perp = 0.20$, there is a sharp coherence peak at the gap edge and weight in the peak increases with increasing $t_\perp$ reaching a maximum at $t_\perp = 0.35$. In figure 4.2, the diagonal component of the spectral functions of both the interacting and non-interacting planes are shown for higher values of $t_\perp$. The left panel represents the spectral function of the interacting plane and right panel represents the spectral function of the non-interacting plane. At $t_\perp = 0.60$, the coherence peak at gap edge in both interacting and interacting planes completely vanishes and both planes become metallic. Further increasing $t_\perp$, both interacting and non-interacting spectral functions become gapped. The nature of this gap, that occurs at large $t_\perp$ will be discussed later. The spectral gap increases with increasing $t_\perp$.

4.4.2 Superconducting order parameter (Φ)

Superconducting order is characterized by a finite value of Φ, hence this is a measure of the strength of the pairing of electrons of opposite momentum and spin. The Φ for both planes is defined in equations 4.12 and 4.14. In the left panel of figure 4.3, Φ vs $t_\perp$ for both interacting and non-interacting planes is shown. The Φ of interacting plane decreases monotonically with increases $t_\perp$ and beyond a critical value of $t_{c\perp} = t_\perp \sim 0.6$, it completely vanishes and interacting plane becomes

non-superconducting. In the non-interacting plane beyond $t_\perp \sim 0.1$ Φ is non zero, indicating that superconductivity is induced in the non-interacting plane. Beyond $t_\perp \sim 0.1$, Φ increases with increasing $t_\perp$ and after a certain value of $t_\perp \sim 0.35$, Φ decreases with increases $t_\perp$ and beyond $t_{c\perp} = t_\perp \sim 0.6$, it completely vanishes, and non-interacting plane also becomes non-superconducting.
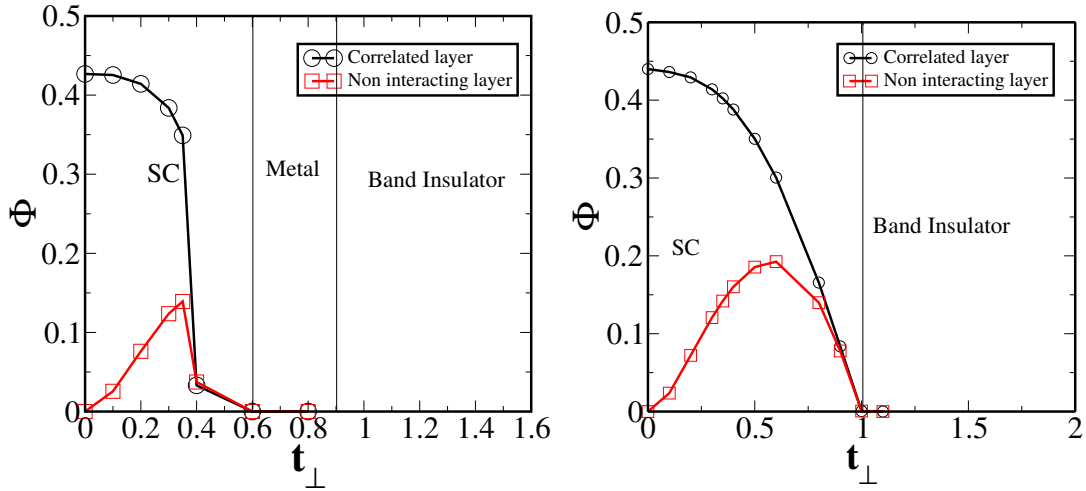

Figure 4.3: Order parameter – Left panel : IPTSC result; Right panel : BdGMF result.

4.4.3 Nature of the Spectral gap

As we see that Φ is finite for $t_\perp < 0.6$, indicating that the nature of the spectral gap for $t_\perp < 0.6$ in figures 4.1 will be superconducting. In the figures 4.2, since $t_\perp > t_{c\perp}$, the Φ must be zero, and hence the system is a simple band insulator.

4.4.4 Comparison of IPTSC and BdGMF Results

To understand the effects of dynamical fluctuations over the static mean field, Φ vs $t_\perp$ within the BdGMF is shown in the right panel of figure 4.3 for both interacting and non-interacting planes. Left panel represents the IPTSC result and the right panel represents the BdGMF result. In both IPTSC and BdGMF framework, Φ for both interacting and non-interacting planes vanishes beyond a critical value of $t_\perp = t_{c\perp}$. This critical value of inter-planar hopping is higher in the BdGMF than in the IPTSC

method. In the BdGMF framework, the superconducting phase continuously goes to insulating phase beyond $t_{c\perp}$ and the intermediate metallic phase is not observed. While in the IPTSC framework, in both the interacting and non-interacting planes, the system first goes from superconductor to metallic phase and subsequently with increasing $t_\perp$, both planes become insulating. Thus dynamical fluctuations strongly modifies the static mean field results.

4.5 Conclusions

In this chapter, we have studied a bilayer attractive Hubbard model by combining DMFT and IPTSC at half filling. We have computed spectral functions and superconducting order parameter for different value of interplanar hopping. Superconductivity is induced in non-interacting layer due to proximity to superconducting plane, and beyond a critical value of interplanar hopping, both planes become non-superconducting. Our results are very similar to a recent determinantal quantum Monte-Carlo study [20] of a bilayer-AHM on finite-size lattices, in terms of the dependence of the order parameter on the $t_\perp$. However, it is not clear that, the intervening metallic phase and the subsequent insulating phase shown in figure 4.3, are also found by the DQMC work. To understand the effect of dynamical fluctuation over static mean field, we have computed the superconducting order parameter in BdGMF approach. In the static mean field approach, the intervening metallic phase is not observed, thus dynamical fluctuations play a very important role over static mean field.

Bibliography

[1] Andreev A F 1964 Zh. Eksp. Teor. Fiz. **46** 1823.

[2] Werthamer N R 1963 Phys. Rev. **132** 2440.

[3] de Gennes P G 1964 Rev. Mod. Phys. **36** 225.

[4] Yakov Fominov 2003 arXiv:cond-mat/0311359.

[5] Jinho Kim, Yong-Joo Doh, K. Char, Hyeonjin Doh, Han-Yong Choi 2005 Phys. Rev. B **71** 214519.

[6] Hiroki Yamazaki, Nic Shannon and Hidenori Takagi 2006 Phys. Rev. B **73** 094507.

[7] Truscott A D, Dynes R C and Schneemeyer L F 1999 Phys. Rev. Lett. **83** 1014-1017.

[8] Kawaguchi K and Sohma M 1992 Phys. Rev. B **46** 14722.

[9] Verbanck G, Potter C D, Metlushko V, Schad R, Mosh-chalkov V V and Bruynseraede Y 1998 Phys. Rev. B **57** 6029.

[10] Mühge Th, Theis-Bröhl K, Westerholt K, Zabel H, Garif'yanov N N, Goryunov Yu V, Garifullin I A and Kha-liullin G G 1998 Phys. Rev. B **57** 5071.

[11] Strunk C, Sürgers C, Paschen U and Löhneysen H V 1994 Phys. Rev. B **49** 4053.

[12] Jiang J S, Davidovic D, Daniel H Reich and Chien C L 1995 Phys. Rev. Lett. **74** 314.

[13] Wong H K, Jin B Y, Yang H Q, Ketterson J B and Hilliard J E 1986 J. Low Temp. Phys. **63** 307.

[14] Koorevaar P, Suzuki Y, Coehoorn R and Aarts J 1994 Phys. Rev. B **49** 441.

[15] Tagirov L R, Garifullin I A, Garif'yanov N N, Khle-bnikov S Ya , Tikhonov D A, Westerholt K and Zabel H 2002 J. Magn. Magn. Mater. **240** 577.

[16] Aarts J, Geers J M E, Brück E, Golubov A A and Coe-hoorn R 1997 Phys. Rev. B **56** 2779.

[17] Lazar L, Westerholt K, Zabel H, Tagirov L R, Goryunov Yu V, Garifyanov N N and Garifullin I A 2000 Phys. Rev. B **61** 3711.

[18] Goto H 2003 Physica B **329-333** 1425.

[19] Sefrioui Z, Arias D, Peña V, Villegas J E, Varela M, Prieto P, Leòn C, Martinez J L and Santa-maria J 2003 Phys. Rev. B **67** 214511.

[20] Aleksander Zujev, Richard T Scalettar, George G Batrouni and Pinaki Sengupta 2012 arXiv:1212.2727.

[21] Georges A, Kotliar G, Krauth W and Rozenberg M J 1996 Rev. Mod. Phys. **68** 13.

[22] Kotliar G and Vollhardt D 2004 Physics Today **57** 53-59.

[23] Vollhardt D AIP Conference Proceedings 2010 **1297** 339.

[24] Garg A, Krishnamurthy H R and Randeria M Phys. Rev. B 2005 **72** 024517.

[25] Masaru Sakaida, Kazuto Noda and Norio Kawakami J. Phys. Soc. Japan 2013 **82** 074715.

[26] Naushad Ahmad Kamar, Vidhyadhiraja N S 2013 arXiv:1309.7224.

Appendix A

A.1 Calculation of second order diagonal part of self energy

Second order diagonal self energy is given by

$$\Sigma^{(2)}(\omega^+) = U^2 \int_{-\infty}^{\infty} \prod_{i=1}^{i=3} d\varepsilon_i [\rho_1(\varepsilon_1)\rho_2(\varepsilon_2)\rho_2(\varepsilon_3) - \rho_3(\varepsilon_1)\rho_2(\varepsilon_2)\rho_3(\varepsilon_3)][f(\varepsilon_1)f(-\varepsilon_2)f(\varepsilon_3) +$$

$$f(-\varepsilon_1)f(\varepsilon_2)f(-\varepsilon_3)]\frac{1}{\omega^+ - \varepsilon_1 + \varepsilon_2 + \varepsilon_3} \quad \text{(A.1)}$$

$$\rho_1 = -\text{Im}\frac{\mathscr{G}_{11}}{\pi}, \ \rho_2 = -\text{Im}\frac{\mathscr{G}_{22}}{\pi}, \ \rho_3 = -\text{Im}\frac{\mathscr{G}_{12}}{\pi} \quad \text{(A.2)}$$

The imaginary part of $\Sigma^{(2)}(\omega^+)$ is given by

$$\mathscr{D}_{\Sigma^{(2)}(\omega^+)} = -\text{Im}\frac{\Sigma^{(2)}(\omega^+)}{\pi} \quad \text{(A.3)}$$

$$\mathscr{D}_{\Sigma^{(2)}(\omega)} = U^2 \int_{-\infty}^{\infty} \prod_{i=1}^{i=3} d\varepsilon_i [\rho_1(\varepsilon_1)\rho_2(\varepsilon_2)\rho_2(\varepsilon_3) - \rho_3(\varepsilon_1)\rho_2(\varepsilon_2)$$

$$\rho_3(\varepsilon_3)][f(\varepsilon_1)f(-\varepsilon_2)f(\varepsilon_3) + f(-\varepsilon_1)f(\varepsilon_2)f(-\varepsilon_3)]\delta(\omega - \varepsilon_1 + \varepsilon_2 - \varepsilon_3) \quad \text{(A.4)}$$

$$\mathscr{D}_{\Sigma^{(2)}(\omega)} = U^2 \int_{-\infty}^{\infty} \prod_{i=1}^{i=2} d\varepsilon_i [\rho_1(\varepsilon_1)\rho_2(\varepsilon_2)\rho_2(\omega - \varepsilon_1 + \varepsilon_2) - \rho_3(\varepsilon_1)\rho_2(\varepsilon_2)$$
$$\rho_3(\omega - \varepsilon_1 + \varepsilon_2)][f(\varepsilon_1)f(-\varepsilon_2)f(\omega - \varepsilon_1 + \varepsilon_2) + f(-\varepsilon_1)f(\varepsilon_2)f(-\omega + \varepsilon_1 - \varepsilon_2)] \tag{A.5}$$

Now changing ε_1 to $-\varepsilon_1$, we get,

$$\mathscr{D}_{\Sigma^{(2)}(\omega)} = U^2 \int_{-\infty}^{\infty} \prod_{i=1}^{i=2} d\varepsilon_i [\rho_1(-\varepsilon_1)\rho_2(\varepsilon_2)\rho_2(\omega + \varepsilon_1 + \varepsilon_2) - \rho_3(-\varepsilon_1)\rho_2(\varepsilon_2)$$
$$\rho_3(\omega + \varepsilon_1 + \varepsilon_2)][f(-\varepsilon_1)f(-\varepsilon_2)f(\omega + \varepsilon_1 + \varepsilon_2) + f(\varepsilon_1)f(\varepsilon_2)f(-\omega - \varepsilon_1 - \varepsilon_2)] \tag{A.6}$$

$$\mathscr{D}_{\Sigma^{(2)}(\omega)} = U^2 \int_{-\infty}^{\infty} \prod_{i=1}^{i=2} d\varepsilon_i [\rho_1(-\varepsilon_1)\rho_2(\varepsilon_2)\rho_2(\omega + \varepsilon_1 + \varepsilon_2)f(-\varepsilon_1)f(-\varepsilon_2)f(\omega + \varepsilon_1 + \varepsilon_2) + \rho_1(-\varepsilon_1)$$
$$\rho_2(\varepsilon_2)\rho_2(\omega + \varepsilon_1 + \varepsilon_2)f(\varepsilon_1)f(\varepsilon_2)f(-\omega - \varepsilon_1 - \varepsilon_2) - \rho_3(-\varepsilon_1)\rho_2(\varepsilon_2)\rho_3(\omega + \varepsilon_1 + \varepsilon_2)f(-\varepsilon_1)f(-\varepsilon_2)$$
$$f(\omega + \varepsilon_1 + \varepsilon_2) - \rho_3(-\varepsilon_1)\rho_2(\varepsilon_2)\rho_3(\omega + \varepsilon_1 + \varepsilon_2)f(\varepsilon_1)f(\varepsilon_2)f(-\omega - \varepsilon_1 - \varepsilon_2)] \tag{A.7}$$

Now define $\mathscr{D}_{\Sigma_1^{(2)}(\omega)}$ as

$$\mathscr{D}_{\Sigma_1^{(2)}(\omega)} = U^2 \int_{-\infty}^{\infty} \prod_{i=1}^{i=2} d\varepsilon_i [\rho_1(-\varepsilon_1)\rho_2(\varepsilon_2)\rho_2(\omega + \varepsilon_1 + \varepsilon_2)f(-\varepsilon_1)f(-\varepsilon_2)f(\omega + \varepsilon_1 + \varepsilon_2)$$

$$= U^2 \int_{-\infty}^{\infty} d\varepsilon_1 \rho_1(-\varepsilon_1)f(-\varepsilon_1) \int_{-\infty}^{\infty} d\varepsilon_2 [\rho_2(\varepsilon_2)f(-\varepsilon_2)\rho_2(\omega + \varepsilon_1 + \varepsilon_2)f(\omega + \varepsilon_1 + \varepsilon_2)] \tag{A.8}$$

Now define χ_1 as

$$\chi_1(\varepsilon) = \int_{-\infty}^{\infty} d\varepsilon_2 [\rho_2(\varepsilon_2)f(-\varepsilon_2)\rho_2(\varepsilon + \varepsilon_2)f(\varepsilon + \varepsilon_2)] \tag{A.9}$$

$$\mathscr{D}_{\Sigma_1^{(2)}(\omega)} = U^2 \int_{-\infty}^{\infty} d\varepsilon_1 \rho_1(-\varepsilon_1)f(-\varepsilon_1)\chi_1(\varepsilon_1 + \omega) \tag{A.10}$$

Now define $\mathscr{D}_{\Sigma_2^{(2)}(\omega)}$ as

$$\mathscr{D}_{\Sigma_2^{(2)}(\omega)} = U^2 \int_{-\infty}^{\infty} \prod_{i=1}^{i=2} d\varepsilon_i \rho_1(-\varepsilon_1)\rho_2(\varepsilon_2)\rho_2(\omega+\varepsilon_1+\varepsilon_2)f(\varepsilon_1)f(\varepsilon_2)f(-\omega-\varepsilon_1-\varepsilon_2) \tag{A.11}$$

Now define χ_2 as

$$\chi_2(-\varepsilon) = \int_{-\infty}^{\infty} d\varepsilon_2 [\rho_2(\varepsilon_2)f(\varepsilon_2)f(\varepsilon-\varepsilon_2)\rho_2(-\varepsilon+\varepsilon_2)] \tag{A.12}$$

Now replacing ε_2 to $\varepsilon + \varepsilon_2$, we get

$$= \int_{-\infty}^{\infty} d\varepsilon_2 [\rho_2(\varepsilon_2+\varepsilon)f(\varepsilon_2+\varepsilon)f(-\varepsilon_2)\rho_2(\varepsilon_2)] \tag{A.13}$$

$$\chi_2(-\varepsilon) = \chi_1(\varepsilon)$$

$$\mathscr{D}_{\Sigma_2^{(2)}(\omega)} = U^2 \int_{-\infty}^{\infty} d\varepsilon_1 \rho_1(-\varepsilon_1)f(\varepsilon_1)\chi_1(-\omega-\varepsilon_1) \tag{A.14}$$

Now define $\mathscr{D}_{\Sigma_3^{(2)}(\omega)}$ as

$$\mathscr{D}_{\Sigma_3^{(2)}(\omega)} = U^2 \int_{-\infty}^{\infty} \prod_{i=1}^{i=2} d\varepsilon_i \rho_3(-\varepsilon_1)\rho_2(\varepsilon_2)\rho_3(\omega+\varepsilon_1+\varepsilon_2)f(-\varepsilon_1)f(-\varepsilon_2)f(\omega+\varepsilon_1+\varepsilon_2)$$

$$= U^2 \int_{-\infty}^{\infty} d\varepsilon_1 \rho_3(-\varepsilon_1)f(-\varepsilon_1) \int_{-\infty}^{\infty} d\varepsilon_2 [\rho_2(\varepsilon_2)f(-\varepsilon_2)\rho_3(\omega+\varepsilon_1+\varepsilon_2)f(\omega+\varepsilon_1+\varepsilon_2)]$$

Now define χ_3 as

$$\chi_3(\varepsilon) = \int_{-\infty}^{\infty} d\varepsilon_2 [\rho_2(\varepsilon_2)f(-\varepsilon_2)\rho_3(\varepsilon+\varepsilon_2)f(\varepsilon+\varepsilon_2)]$$

$$\mathscr{D}_{\Sigma_3^{(2)}(\omega)} = \int_{-\infty}^{\infty} d\varepsilon_1 \rho_3(-\varepsilon_1)f(-\varepsilon_1)\chi_3(\omega+\varepsilon_1) \tag{A.15}$$

Now define $\mathscr{D}_{\Sigma_4^{(2)}(\omega)}$

$$\mathscr{D}_{\Sigma_4^{(2)}(\omega)} = U^2 \int_{-\infty}^{\infty} \prod_{i=1}^{i=2} d\varepsilon_i \rho_3(-\varepsilon_1)\rho_2(\varepsilon_2)\rho_3(\omega+\varepsilon_1+\varepsilon_2)f(\varepsilon_1)f(\varepsilon_2)f(-\omega-\varepsilon_1-\varepsilon_2)$$

$$= \int_{-\infty}^{\infty} d\varepsilon_1 f(\varepsilon_1)\rho_3(-\varepsilon_1) \int_{-\infty}^{\infty} d\varepsilon_2 [\rho_2(\varepsilon_2)f(\varepsilon_2)\rho_3(\omega+\varepsilon_1+\varepsilon_2)f(-\omega-\varepsilon_1-\varepsilon_2)]$$

Now define χ_4 as

$$\chi_4(\varepsilon) = \int_{-\infty}^{\infty} d\varepsilon_2 [\rho_2(\varepsilon_2)f(\varepsilon_2)\rho_3(\varepsilon+\varepsilon_2)f(-\varepsilon-\varepsilon_2)]$$

$$\mathscr{D}_{\Sigma_4^{(2)}(\omega)} = \int_{-\infty}^{\infty} d\varepsilon_1 f(\varepsilon_1)\rho_3(-\varepsilon_1)\chi_4(\omega+\varepsilon_1) \tag{A.16}$$

By using equation A.8, A.11, A.15, and A.16 , $\mathscr{D}_{\Sigma^{(2)}(\omega)}$ can be written as,

$$\mathscr{D}_{\Sigma^{(2)}(\omega)} = \mathscr{D}_{\Sigma_1^{(2)}(\omega)} + \mathscr{D}_{\Sigma_2^{(2)}(\omega)} - \mathscr{D}_{\Sigma_3^{(2)}(\omega)} - \mathscr{D}_{\Sigma_4^{(2)}(\omega)} \tag{A.17}$$

The real part of $\Sigma^{(2)}(\omega^+)$ is given by using Kramers-Kronig transformation of $\mathscr{D}_{\Sigma^{(2)}(\omega)}$,

$$Real(\Sigma^{(2)}(\omega)) = \int_{-\infty}^{\infty} d\varepsilon \frac{\mathscr{D}_{\Sigma^{(2)}(\omega)}}{\omega-\varepsilon} \tag{A.18}$$

Finally self energy is given by

$$\Sigma^{(2)}(\omega) = Real(\Sigma^{(2)}(\omega)) - i\pi\mathscr{D}_{\Sigma^{(2)}(\omega)} \tag{A.19}$$

A.2 Calculation of second order off diagonal part of self energy

Second order off-diagonal self energy is given by,

$$
S^{(2)}(\omega) = U^2 \int_{-\infty}^{\infty} \prod_{i=1}^{i=3} d\varepsilon_i [\rho_3(\varepsilon_1)\rho_3(\varepsilon_2)\rho_3(\varepsilon_3) - \rho_1(\varepsilon_1)\rho_3(\varepsilon_2)\rho_2(\varepsilon_3)][f(\varepsilon_1)f(-\varepsilon_2)f(\varepsilon_3) +
$$
$$
f(-\varepsilon_1)f(\varepsilon_2)f(-\varepsilon_3)]\frac{1}{\omega^+ - \varepsilon_1 + \varepsilon_2 + \varepsilon_3} \quad \text{(A.20)}
$$

Imaginary part of $S^{(2)}(\omega)$ is given by

$$
\mathscr{D}_{S^{(2)}(\omega)} = -\text{Im}\frac{S^{(2)}(\omega)}{\pi} \quad \text{(A.21)}
$$

$$
\mathscr{D}_{S^{(2)}(\omega)} = U^2 \int_{-\infty}^{\infty} \prod_{i=1}^{i=3} d\varepsilon_i [\rho_3(\varepsilon_1)\rho_3(\varepsilon_2)\rho_3(\varepsilon_3) - \rho_1(\varepsilon_1)\rho_3(\varepsilon_2)
$$
$$
\rho_2(\varepsilon_3)][f(\varepsilon_1)f(-\varepsilon_2)f(\varepsilon_3) + f(-\varepsilon_1)f(\varepsilon_2)f(-\varepsilon_3)\delta(\omega - \varepsilon_1 + \varepsilon_2 - \varepsilon_3)] \quad \text{(A.22)}
$$

Now replacing ε_1 to $-\varepsilon_1$, we get

$$
\mathscr{D}_{S^{(2)}(\omega)} = U^2 \int_{-\infty}^{\infty} \prod_{i=1}^{i=2} d\varepsilon_i [\rho_3(-\varepsilon_1)\rho_3(\varepsilon_2)\rho_3(\omega + \varepsilon_1 + \varepsilon_2) - \rho_1(-\varepsilon_1)\rho_3(\varepsilon_2)
$$
$$
\rho_2(\omega + \varepsilon_1 + \varepsilon_2)][f(-\varepsilon_1)f(-\varepsilon_2)f(\omega + \varepsilon_1 + \varepsilon_2) + f(\varepsilon_1)f(\varepsilon_2)f(-\omega - \varepsilon_1 - \varepsilon_2)] \quad \text{(A.23)}
$$

Now define $\mathscr{D}_{S_1^{(2)}(\omega)}$ as

$$
\mathscr{D}_{S_1^{(2)}(\omega)} = U^2 \int_{-\infty}^{\infty} \prod_{i=1}^{i=2} d\varepsilon_i [\rho_3(-\varepsilon_1)\rho_3(\varepsilon_2)\rho_3(\omega + \varepsilon_1 + \varepsilon_2)f(-\varepsilon_1)f(-\varepsilon_2)f(\omega + \varepsilon_1 + \varepsilon_2)]
$$

$$
= U^2 \int_{-\infty}^{\infty} d\varepsilon_1 \rho_3(-\varepsilon_1)f(-\varepsilon_1) \int_{-\infty}^{\infty} d\varepsilon_2 [\rho_3(\varepsilon_2)f(-\varepsilon_2)\rho_3(\omega + \varepsilon_1 + \varepsilon_2)f(\omega + \varepsilon_1 + \varepsilon_2)]
$$

Now define χ_5 as

$$
\chi_5(\varepsilon) = \int_{-\infty}^{\infty} d\varepsilon_2 [\rho_3(\varepsilon_2)f(-\varepsilon_2)\rho_3(\varepsilon + \varepsilon_2)f(\varepsilon + \varepsilon_2)] \quad \text{(A.24)}
$$

$$\mathscr{D}_{S_1^{(2)}(\omega)} = U^2 \int_{-\infty}^{\infty} d\varepsilon_1 \rho_3(-\varepsilon_1) f(-\varepsilon_1) \chi_5(\omega + \varepsilon_1) \tag{A.25}$$

Now define $\mathscr{D}_{S_2^{(2)}(\omega)}$ as

$$\mathscr{D}_{S_2^{(2)}(\omega)} = U^2 \int_{-\infty}^{\infty} \prod_{i=1}^{i=2} d\varepsilon_i [\rho_3(-\varepsilon_1)\rho_3(\varepsilon_2)\rho_3(\omega + \varepsilon_1 + \varepsilon_2) f(\varepsilon_1) f(\varepsilon_2) f(-\omega - \varepsilon_1 - \varepsilon_2)]$$

$$= U^2 \int_{-\infty}^{\infty} d\varepsilon_1 \rho_3(-\varepsilon_1) f(\varepsilon_1) \int_{-\infty}^{\infty} d\varepsilon_2 [\rho_3(\varepsilon_2) f(\varepsilon_2) \rho_3(\omega + \varepsilon_1 + \varepsilon_2) f(-\omega - \varepsilon_1 - \varepsilon_2)]$$

Now define χ_6 as

$$\chi_6(\varepsilon) = \int_{-\infty}^{\infty} d\varepsilon_2 [\rho_3(\varepsilon_2) f(\varepsilon_2) \rho_3(\varepsilon + \varepsilon_2) f(-\varepsilon - \varepsilon_2)]$$

$$\chi_6(-\varepsilon) = \int_{-\infty}^{\infty} d\varepsilon_2 [\rho_3(\varepsilon_2) f(\varepsilon_2) \rho_3(-\varepsilon + \varepsilon_2) f(\varepsilon - \varepsilon_2)]$$

Now replace ε_2 by $\varepsilon_2 + \varepsilon$, we get

$$\chi_6(-\varepsilon) = \int_{-\infty}^{\infty} d\varepsilon_2 [\rho_3(\varepsilon_2 + \varepsilon) f(\varepsilon_2 + \varepsilon) \rho_3(\varepsilon_2) f(-\varepsilon_2)] = \chi_5(\varepsilon)$$

$$\mathscr{D}_{S_2^{(2)}(\omega)} = U^2 \int_{-\infty}^{\infty} d\varepsilon_1 \rho_3(-\varepsilon_1) f(\varepsilon_1) \chi_5(-\omega - \varepsilon_1) \tag{A.26}$$

Now define $\mathscr{D}_{S_3^{(2)}(\omega)}$ as

$$\mathscr{D}_{S_3^{(2)}(\omega)} = U^2 \int_{-\infty}^{\infty} \prod_{i=1}^{i=2} d\varepsilon_i [\rho_1(-\varepsilon_1)\rho_3(\varepsilon_2)\rho_2(\omega + \varepsilon_1 + \varepsilon_2) f(-\varepsilon_1) f(-\varepsilon_2) f(\omega + \varepsilon_1 + \varepsilon_2)]$$

$$= U^2 \int_{-\infty}^{\infty} d\varepsilon_1 \rho_1(-\varepsilon_1) f(-\varepsilon_1) \int_{-\infty}^{\infty} d\varepsilon_2 [\rho_3(\varepsilon_2) f(-\varepsilon_2) \rho_2(\omega + \varepsilon_1 + \varepsilon_2) f(\omega + \varepsilon_1 + \varepsilon_2)]$$

Now define χ_7 as

$$\chi_7(\varepsilon) = \int_{-\infty}^{\infty} d\varepsilon_2 [\rho_3(\varepsilon_2) f(-\varepsilon_2) \rho_2(\varepsilon + \varepsilon_2) f(\varepsilon + \varepsilon_2)]$$

$$\mathscr{D}_{S_3^{(2)}(\omega)} = U^2 \int_{-\infty}^{\infty} d\varepsilon_1 \rho_1(-\varepsilon_1) f(-\varepsilon_1) \chi_7(\varepsilon_1 + \omega) \tag{A.27}$$

Now define $\mathscr{D}_{S_4^{(2)}(\omega)}$ as

$$\mathscr{D}_{S_4^{(2)}(\omega)} = U^2 \int_{-\infty}^{\infty} \prod_{i=1}^{i=2} d\varepsilon_i [\rho_1(-\varepsilon_1) \rho_3(\varepsilon_2) \rho_2(\omega + \varepsilon_1 + \varepsilon_2) f(\varepsilon_1) f(\varepsilon_2) f(-\omega - \varepsilon_1 - \varepsilon_2)]$$

$$= U^2 \int_{-\infty}^{\infty} d\varepsilon_1 \rho_1(-\varepsilon_1) f(\varepsilon_1) \int_{-\infty}^{\infty} d\varepsilon_2 [\rho_3(\varepsilon_2) \rho_2(\omega + \varepsilon_1 + \varepsilon_2) f(\varepsilon_2) f(-\omega - \varepsilon_1 - \varepsilon_2)]$$

Now define χ_8 as

$$\chi_8(\varepsilon) = \int_{-\infty}^{\infty} d\varepsilon_2 [\rho_3(\varepsilon_2) \rho_2(\varepsilon + \varepsilon_2) f(\varepsilon_2) f(-\varepsilon - \varepsilon_2)]$$

$$\mathscr{D}_{S_4^{(2)}(\omega)} = U^2 \int_{-\infty}^{\infty} d\varepsilon_1 \rho_1(-\varepsilon_1) f(\varepsilon_1) \chi_8(\varepsilon_1 + \omega) \tag{A.28}$$

By using equation A.25, A.26, A.27, and A.28 , $\mathscr{D}_{S^{(2)}(\omega)}$ is given by

$$\mathscr{D}_{S^{(2)}(\omega)} = \mathscr{D}_{S_1^{(2)}(\omega)} + \mathscr{D}_{S_2^{(2)}(\omega)} - \mathscr{D}_{S_3^{(2)}(\omega)} - \mathscr{D}_{S_4^{(2)}(\omega)} \tag{A.29}$$

Now by using Kramers-Kronig relation, the real part of $S^2(\omega)$ is given by

$$\mathrm{Re}(S^{(2)}(\omega)) = \int_{-\infty}^{\infty} d\varepsilon \frac{\mathscr{D}_{S^{(2)}(\omega)}}{\omega - \varepsilon} \tag{A.30}$$

$$S^{(2)}(\omega) = \mathrm{Re}(S^{(2)}(\omega)) - i\pi \mathscr{D}_{S^{(2)}(\omega)} \tag{A.31}$$

A.3 Mapping of attractive Hubbard model to repulsive Hubbard model

The attractive Hubbard model (AHM) can be mapped onto repulsive Hubbard model by using appropriate particle-hole(p-h) transformation.

Let us define AHM

$$\mathscr{H} = \sum_{i\sigma} \varepsilon c_{i\sigma}^{\dagger} c_{i\sigma} - t \sum_{\langle ij\sigma \rangle} \left(c_{i\sigma}^{\dagger} c_{j\sigma} + h.c \right) - |U| \sum_{i} n_{i\uparrow} n_{i\downarrow} - \mu \sum_{i\sigma} c_{i\sigma}^{\dagger} c_{i\sigma} \tag{A.32}$$

Now apply following p-h transformation on AHM

$$c_{i\uparrow} \to c_{i\uparrow}$$
$$c_{i\downarrow} \to (-1)^{i} c_{i\downarrow}^{\dagger} \tag{A.33}$$

The transformed Hamiltonian is given by

$$\mathscr{H}_T = \sum_{i} \varepsilon (n_{i\uparrow} - n_{i\downarrow}) + \varepsilon \sum_{i\sigma} 1 - t \sum_{\langle ij\sigma \rangle} \left(c_{i\sigma}^{\dagger} c_{j\sigma} + h.c \right) - |U| \sum_{i} n_{i\uparrow} (1 - n_{i\downarrow}) - $$
$$\mu \sum_{i} (n_{i\uparrow} - n_{i\downarrow}) - \mu \sum_{i\sigma} 1 \tag{A.34}$$

$$\mathscr{H}_T = -t \sum_{\langle ij\sigma \rangle} \left(c_{i\sigma}^{\dagger} c_{j\sigma} + h.c \right) + |U| \sum_{i} n_{i\uparrow} n_{i\downarrow} - (\mu - \varepsilon) \sum_{i} (n_{i\uparrow} - n_{i\downarrow}) $$
$$- (\mu - \varepsilon) \sum_{i\sigma} 1 - |U| \sum_{i} n_{i\uparrow} \tag{A.35}$$

Above Hamiltonian represents repulsive Hubbard model with magnetic field, $(\mu - \varepsilon)$ acts as magnetic field.

Particle number (N_T) in transformed Hamiltonian ($\mathcal{H}_T$) is given by

$$N = \sum_i (n_{i\uparrow} + n_{i\downarrow})$$
$$N_T = \sum_i (n_{i\uparrow} - n_{i\downarrow} + 1)$$
$$= M + N_s \qquad \text{(A.36)}$$

where M is magnetization in original Hamiltonian ($\mathcal{H}$), and N_s is total number of lattice sites.

Magnetization (M_T) in transformed Hamiltonian ($\mathcal{H}_T$) is given by

$$M = \sum_i (n_{i\uparrow} - n_{i\downarrow}) \qquad \text{(A.37)}$$

$$M_T = \sum_i (n_{i\uparrow} + n_{i\downarrow} - 1)$$
$$= N - N_s \qquad \text{(A.38)}$$

Let us consider, $M = 0$, then $N_T = N_s$. If original Hamiltonian is at half filled then $N = N_s$, $M_T = M = 0$, thus half filled attractive Hubbard model with zero magnetization is mapped onto the repulsive Hubbard model with zero magnetization.

If $\mathcal{H}$ is away from half filling, then we can write

$$N = (1 + x)N_s \qquad \text{(A.39)}$$

where x is doping parameter.

$$M_T = xN_s \qquad \text{(A.40)}$$

Thus away from half- filled attractive Hubbard model is equivalent to repulsive Hubbard model with finite magnetization.
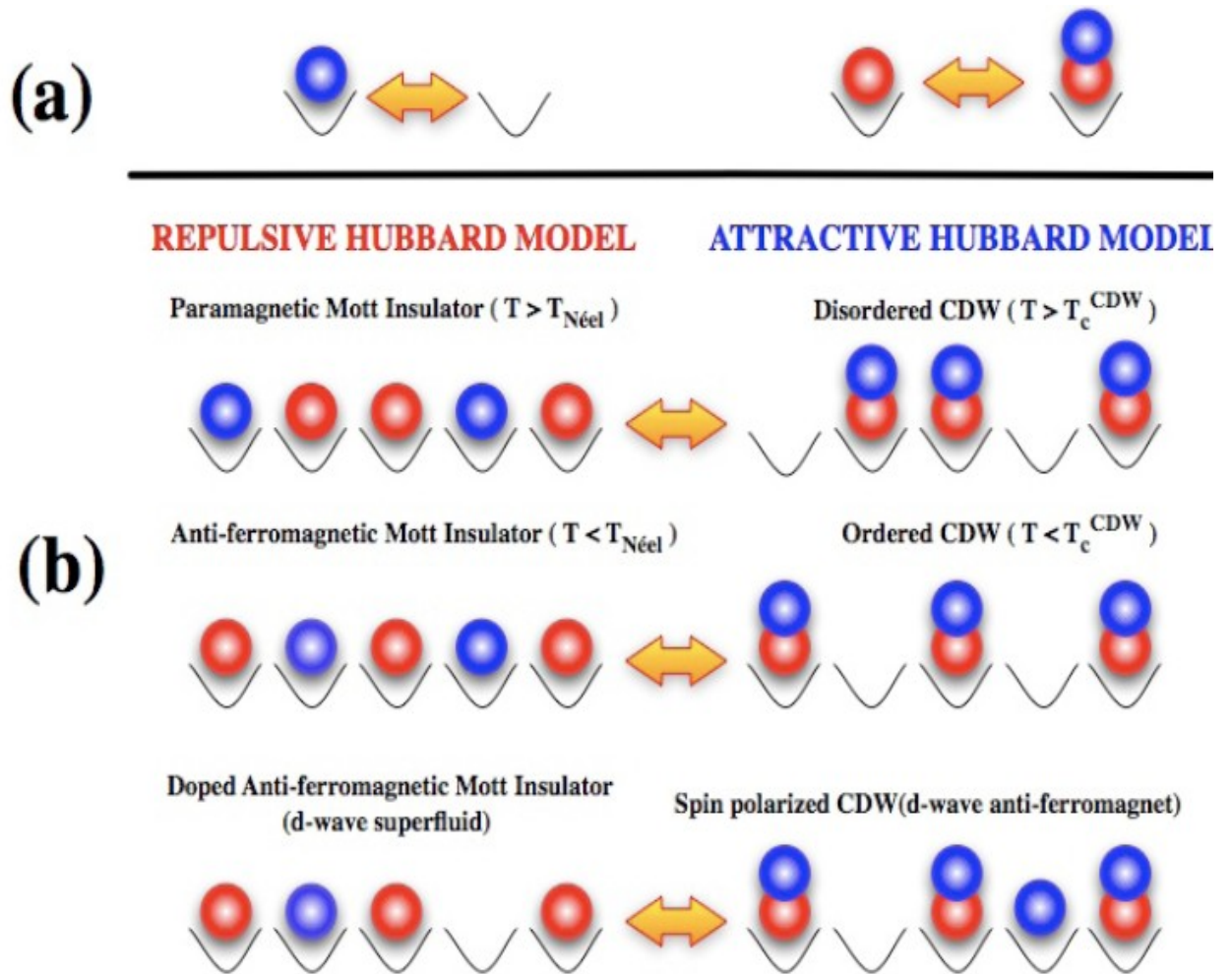
Figure A.1: Schematic diagram of how particle-hole transformation works. Blue stands for spin down and red stands for spin up electrons. Spin down electron transforms to vacant site, vacant site transforms to spin down electron, spin up electron transforms to Cooper pair and Copper pair transforms to spin up electron by p-h transformation (From Ref. [1]).

A.4 Calculation of factor $\hat{A}$

Factor $\hat{A}$ is calculated by imposing the condition that IPTSC is exact in high frequency limit.

Second order selfenergy in high frequency limit is given by

$$\Sigma^{(2)}(\omega \to \infty) = U^2 \int_{-\infty}^{\infty} \prod_{j=1}^{3} d\omega_j \frac{g_1(\omega_1, \omega_2, \omega_3) N(\omega_1, \omega_2, \omega_3)}{\omega^+}$$

and

$$S^{(2)}(\omega \to \infty) = U^2 \int_{-\infty}^{\infty} \prod_{j=1}^{3} d\omega_j \frac{g_2(\omega_1, \omega_2, \omega_3) N(\omega_1, \omega_2, \omega_3)}{\omega^+} \tag{A.41}$$

$$N(\omega_1, \omega_2, \omega_3) = f(\omega_1)f(-\omega_2)f(\omega_3) + f(-\omega_1)f(\omega_2)f(-\omega_3)$$

$$g_1(\omega_1, \omega_2, \omega_3) = \tilde{\rho}_{11}(\omega_1)\tilde{\rho}_{22}(\omega_2)\tilde{\rho}_{22}(\omega_3) - \tilde{\rho}_{12}(\omega_1)\tilde{\rho}_{22}(\omega_2)\tilde{\rho}_{12}(\omega_3)$$

$$g_2(\omega_1, \omega_2, \omega_3) = \tilde{\rho}_{12}(\omega_1)\tilde{\rho}_{12}(\omega_2)\tilde{\rho}_{12}(\omega_3) - \tilde{\rho}_{11}(\omega_1)\tilde{\rho}_{12}(\omega_2)\tilde{\rho}_{22}(\omega_3) \tag{A.42}$$

$$\Sigma^{(2)}(\omega \to \infty) = \frac{U^2}{\omega^+} \int_{-\infty}^{\infty} \prod_{j=1}^{3} d\omega_j [\tilde{\rho}_{11}(\omega_1)\tilde{\rho}_{22}(\omega_2)\tilde{\rho}_{22}(\omega_3)f(\omega_1)$$

$$f(-\omega_2)f(\omega_3) + \tilde{\rho}_{11}(\omega_1)\tilde{\rho}_{22}(\omega_2)\tilde{\rho}_{22}(\omega_3)f(-\omega_1)f(\omega_2)f(-\omega_3) - \tilde{\rho}_{12}(\omega_1)\tilde{\rho}_{22}(\omega_2)$$

$$\tilde{\rho}_{12}(\omega_3)f(\omega_1)f(-\omega_2)f(\omega_3) - \tilde{\rho}_{12}(\omega_1)\tilde{\rho}_{22}(\omega_2)\tilde{\rho}_{12}(\omega_3)f(-\omega_1)f(\omega_2)f(-\omega_3)]$$

$$= \frac{U^2}{\omega^+} \left[\frac{n_0}{2}\frac{n_0}{2}(1 - \frac{n_0}{2}) + (1 - \frac{n_0}{2})(1 - \frac{n_0}{2})\frac{n_0}{2} - \Phi_0\frac{n_0}{2}\Phi_0 - \Phi_0(1 - \frac{n_0}{2})\Phi_0 \right]$$

$$= \frac{U^2}{\omega^+} \left[\frac{n_0^2}{4} - \frac{n_0^3}{8} + \frac{n_0}{2} + \frac{n_0^3}{8} - \frac{n_0^2}{2} - \Phi_0^2 \right]$$

$$= \frac{U^2}{\omega^+} \left[\frac{n_0}{2} - \frac{n_0^2}{4} - \Phi_0^2 \right] \tag{A.43}$$

$$S^{(2)}(\omega \to \infty) = \frac{U^2}{\omega^+} \int_{-\infty}^{\infty} \prod_{j=1}^{3} d\omega_j [\tilde{\rho}_{12}(\omega_1)\tilde{\rho}_{12}(\omega_2)\tilde{\rho}_{12}(\omega_3)f(\omega_1)f(-\omega_2)f(\omega_3) + \tilde{\rho}_{12}(\omega_1)\tilde{\rho}_{12}(\omega_2)$$

$$\tilde{\rho}_{12}(\omega_3)f(-\omega_1)f(\omega_2)f(-\omega_3) - \tilde{\rho}_{11}(\omega_1)\tilde{\rho}_{12}(\omega_2)$$

$$\tilde{\rho}_{22}(\omega_3)f(\omega_1)f(-\omega_2)f(\omega_3) - \tilde{\rho}_{11}(\omega_1)\tilde{\rho}_{12}(\omega_2)\tilde{\rho}_{22}(\omega_3)f(-\omega_1)f(\omega_2)f(-\omega_3)]$$

$$= \frac{U^2}{\omega^+}\left[-\Phi_0^3 + \Phi_0^3 + \frac{n_0}{2}\Phi_0(1-\frac{n_0}{2}) - (1-\frac{n_0}{2})\Phi_0\frac{n_0}{2}\right] = 0$$

$$(A.44)$$

Second order off- diagonal selfenergy vanishes in high frequency limit, implies off-diagonal components of $\hat{A}$ will be zero .

In above calculations, we have used

$$A_{12} = A_{21} = 0 \qquad (A.45)$$

$$\tilde{\rho}_{22}(\omega) = \tilde{\rho}_{11}(-\omega)$$

$$\tilde{\rho}_{12}(-\omega) = -\tilde{\rho}_{12}(\omega)$$

$$\frac{n_0}{2} = \int_{-\infty}^{\infty} d\omega \tilde{\rho}_{11}(\omega)f(\omega)$$

$$1 - \frac{n_0}{2} = \int_{-\infty}^{\infty} d\omega \tilde{\rho}_{11}(-\omega)f(\omega)$$

$$\Phi_0 = \int_{-\infty}^{\infty} d\omega \tilde{\rho}_{12}(\omega)f(\omega)$$

$$-\Phi_0 = \int_{-\infty}^{\infty} d\omega \tilde{\rho}_{12}(-\omega)f(\omega) \qquad (A.46)$$

Let us defined Attractive single impurity Anderson model

$$\mathscr{H}_{imp} = (\varepsilon - \mu)\sum_{\sigma} f_{\sigma}^{\dagger}f_{\sigma} - Un_{\uparrow}^{f}n_{\downarrow}^{f} + \sum_{\vec{k}\sigma} V_{\vec{k}}(c_{\vec{k}\sigma}^{\dagger}f_{\sigma} + h.c) \qquad (A.47)$$

where f represents the annihilation operator of impurity and $c_{\vec{k}}$ represents the annihilation operator of bath.

The impurity Green's function can be written as

$$\hat{G}(\omega) = \int_{-\infty}^{\infty} d\varepsilon \frac{\hat{\rho}_G(\varepsilon)}{\omega^+ - \varepsilon} \tag{A.48}$$

where $\hat{\rho}_G(\varepsilon)$ represents the density of states of lattice. Now $\hat{G}(\omega \to \infty)$ is obtained by expanding $(\omega^+ - \varepsilon)^{-1}$ by using Taylor's expansion

$$\hat{G}(\omega \to \infty) = \frac{1}{\omega^+} \int_{-\infty}^{\infty} d\varepsilon (\hat{\rho}_G(\varepsilon) + \hat{\rho}_G(\varepsilon) \frac{\varepsilon}{\omega^+} + \hat{\rho}_G(\varepsilon) \frac{\varepsilon^2}{\omega^{+2}} + \ldots \ldots) \tag{A.49}$$

Let us defined $\hat{M}^{(n)}$, nth moment of spectral function as

$$\hat{M}^{(n)} = \int_{-\infty}^{\infty} d\varepsilon \varepsilon^n \hat{\rho}_G(\varepsilon) \tag{A.50}$$

$\hat{M}^{(n)}$ in terms of $\mathcal{H}_{imp}$ is given by

$$\hat{M}^{(n)} = \langle \{ [[\Psi, \mathcal{H}_{imp}], \mathcal{H}_{imp}], \ldots n \ times], \Psi^\dagger \} \tag{A.51}$$

where Ψ is two component Nambu spinors, given by

$$\Psi = \begin{bmatrix} f_\uparrow \\ f_\downarrow^\dagger \end{bmatrix}$$

$\hat{M}^{(0)}$ is given by

$$M_{11}^{(0)} = \int_{-\infty}^{\infty} d\varepsilon \rho_G^{11}(\varepsilon) = 1$$
$$M_{12}^{(0)} = \int_{-\infty}^{\infty} d\varepsilon \rho_G^{12}(\varepsilon) = 0$$
$$M_{21}^{(0)} = \int_{-\infty}^{\infty} d\varepsilon \rho_G^{21}(\varepsilon) = 0$$
$$M_{22}^{(0)} = \int_{-\infty}^{\infty} d\varepsilon \rho_G^{22}(\varepsilon) = 1 \tag{A.52}$$

Then $\hat{M}^{(1)}$ is given by

$$\hat{M}^{(1)} = \langle\{[\Psi, \mathscr{H}_{imp}], \Psi^\dagger\}\rangle \tag{A.53}$$

$$
\begin{aligned}
M_{11}^{(1)} &= \langle\{[f_\uparrow, \mathscr{H}_{imp}], f_\uparrow^\dagger\}\rangle \\
M_{12}^{(1)} &= \langle\{[f_\uparrow, \mathscr{H}_{imp}], f_\downarrow\}\rangle \\
M_{21}^{(1)} &= \langle\{[f_\downarrow^\dagger, \mathscr{H}_{imp}], f_\uparrow^\dagger\}\rangle \\
M_{22}^{(1)} &= \langle\{[f_\downarrow^\dagger, \mathscr{H}_{imp}], f_\downarrow\}\rangle
\end{aligned} \tag{A.54}
$$

$$
\begin{aligned}
[f_\uparrow, \mathscr{H}_{imp}] &= (\varepsilon - \mu)[f_\uparrow, \sum_\sigma f_\sigma^\dagger f_\sigma] - U[f_\uparrow, n_\uparrow^f n_\downarrow^f] + \sum_{\vec{k}\sigma} V_{\vec{k}}[f_\uparrow, c_{\vec{k}\sigma}^\dagger f_\sigma + h.c.] \\
&= (\varepsilon - \mu)f_\uparrow - U[f_\uparrow, n_\uparrow^f]n_\downarrow^f + \sum_{\vec{k}} V_{\vec{k}} c_{\vec{k}\uparrow} \\
&= (\varepsilon - \mu)f_\uparrow - U f_\uparrow n_\downarrow^f + \sum_{\vec{k}} V_{\vec{k}} c_{\vec{k}\uparrow} \\
\langle\{[f_\uparrow, \mathscr{H}_{imp}], f_\uparrow^\dagger\}\rangle &= (\varepsilon - \mu) - U\langle n_\downarrow^f\rangle \\
\langle n_\downarrow^f\rangle &= \frac{n}{2} \\
M_{11}^{(1)} &= (\varepsilon - \mu) - U\frac{n}{2}
\end{aligned}
$$

$$\tag{A.55}$$

$$
\begin{aligned}
[f_\uparrow, \mathscr{H}_{imp}] &= (\varepsilon - \mu)f_\uparrow - U f_\uparrow n_\downarrow^f + \sum_{\vec{k}} V_{\vec{k}} c_{\vec{k}\uparrow} \\
\langle\{[f_\uparrow, \mathscr{H}_{imp}], f_\downarrow\}\rangle &= -U\langle\{f_\uparrow n_\downarrow^f, f_\downarrow\} = -U(f_\uparrow n_\downarrow^f f_\downarrow + f_\downarrow f_\uparrow n_\downarrow^f)\rangle \\
&= -U\langle (f_\uparrow f_\downarrow^\dagger f_\downarrow f_\downarrow + f_\downarrow f_\uparrow n_\downarrow^f)\rangle, \ f_\downarrow f_\downarrow = 0 \\
&= -U\langle f_\downarrow f_\uparrow n_\downarrow^f\rangle = U\langle f_\uparrow f_\downarrow n_\downarrow^f\rangle \\
&= U\langle f_\uparrow f_\downarrow f_\downarrow^\dagger f_\downarrow\rangle = U\langle f_\uparrow (1 - f_\downarrow^\dagger f_\downarrow)f_\downarrow\rangle = U\langle f_\uparrow f_\downarrow\rangle \\
&= U\Phi, \ where, \ \Phi = \langle f_\uparrow f_\downarrow\rangle \\
M_{12}^{(1)} &= U\Phi
\end{aligned} \tag{A.56}
$$

67

$$[f_\downarrow^\dagger, \mathscr{H}_{imp}] = -(\varepsilon - \mu)f_\downarrow^\dagger + Un_\uparrow^f f_\downarrow^\dagger - \sum_{\vec{k}} V_{\vec{k}} c_{\vec{k}\downarrow}^\dagger$$

$$\langle \{[f_\downarrow^\dagger, \mathscr{H}_{imp}], f_\downarrow\} \rangle = -(\varepsilon - \mu) + U\langle n_\uparrow^f \rangle, \ \langle n_\uparrow^f \rangle = \frac{n}{2}$$

$$= -(\varepsilon - \mu) + U\frac{n}{2}$$

$$M_{22}^{(1)} = -(\varepsilon - \mu) + U\frac{n}{2}$$

$$\langle \{[f_\downarrow^\dagger, \mathscr{H}_{imp}], f_\uparrow^\dagger\} \rangle = U\langle \{n_\uparrow^f f_\downarrow^\dagger, f_\uparrow^\dagger\} \rangle = U\langle n_\uparrow^f f_\downarrow^\dagger f_\uparrow^\dagger + f_\uparrow^\dagger n_\uparrow^f f_\downarrow^\dagger \rangle = U\langle n_\uparrow^f f_\downarrow^\dagger f_\uparrow^\dagger + f_\uparrow^\dagger f_\uparrow^\dagger f_\uparrow f_\downarrow^\dagger \rangle, \ f_\uparrow^\dagger f_\uparrow^\dagger = 0$$

$$= U\langle n_\uparrow^f f_\downarrow^\dagger f_\uparrow^\dagger \rangle = U\langle f_\downarrow^\dagger n_\uparrow^f f_\uparrow^\dagger \rangle$$

$$= U\langle f_\downarrow^\dagger (1 - f_\uparrow f_\uparrow^\dagger)f_\uparrow^\dagger \rangle = U\langle f_\downarrow^\dagger f_\uparrow^\dagger \rangle$$

$$M_{21}^{(1)} = U\Phi, \ \Phi = \langle f_\downarrow^\dagger f_\uparrow^\dagger \rangle$$

$$(A.57)$$

$$M_{11}^{(2)} = \langle \{[[f_\uparrow, \mathscr{H}_{imp}], \mathscr{H}_{imp}], f_\uparrow^\dagger\} \rangle$$

$$M_{12}^{(2)} = \langle \{[[f_\uparrow, \mathscr{H}_{imp}], \mathscr{H}_{imp}], f_\downarrow\} \rangle$$

$$M_{21}^{(2)} = \langle \{[[f_\downarrow^\dagger, \mathscr{H}_{imp}], \mathscr{H}_{imp}], f_\uparrow^\dagger\} \rangle$$

$$M_{22}^{(2)} = \langle \{[[f_\downarrow^\dagger, \mathscr{H}_{imp}], \mathscr{H}_{imp}], f_\downarrow\} \rangle$$

$$(A.58)$$

$$[f_\uparrow, \mathscr{H}_{imp}], \mathscr{H}_{imp}] = (\varepsilon - \mu)^2 f_\uparrow - 2(\varepsilon - \mu)U f_\uparrow n_\downarrow + U^2 f_\uparrow n_\downarrow - U\sum_{\vec{k}} V_{\vec{k}}[n_\downarrow^f c_{\vec{k}\uparrow} - c_{\vec{k}\uparrow}^\dagger f_\uparrow f_\downarrow + n_\downarrow^f c_{\vec{k}\downarrow} + \sum_k V_{\vec{k}}^2 f_\uparrow]$$

$$\langle \{[[f_\uparrow, \mathscr{H}_{imp}], \mathscr{H}_{imp}], f_\uparrow^\dagger]\} \rangle = (\varepsilon - \mu)^2 - 2U(\varepsilon - \mu)\langle n_\downarrow^f \rangle + U^2 \langle n_\downarrow^f \rangle + \sum_{\vec{k}} V_{\vec{k}}^2$$

$$= (\varepsilon - \mu)^2 - 2U(\varepsilon - \mu)\frac{n}{2} + U^2 \frac{n}{2} + \sum_{\vec{k}} V_{\vec{k}}^2$$

$$M_{11}^{(2)} = (\varepsilon - \mu)^2 - 2U(\varepsilon - \mu)\frac{n}{2} + U^2 \frac{n}{2} + \sum_{\vec{k}} V_{\vec{k}}^2$$

$$M_{22}^{(2)} = (\varepsilon - \mu)^2 - 2U(\varepsilon - \mu)\frac{n}{2} + U^2 \frac{n}{2} - \sum_{\vec{k}} V_{\vec{k}}^2$$

$$M_{12}^{(2)} = -(-2(\varepsilon - \mu)U + U^2)\Phi$$

$$M_{21}^{(2)} = -(-2(\varepsilon - \mu)U + U^2)\Phi$$

$$(A.59)$$

Now for simplicity let us take $\varepsilon = \mu = 0$, then lattice Green's function in high frequency is given by

$$G_{11}(\omega \to \infty) = \frac{1}{\omega^+} - \frac{Un}{2\omega^{+2}} + \sum_{\vec{k}} \frac{V_{\vec{k}}^2 + U^2 n/2}{\omega^{+3}}$$

$$G_{22}(\omega \to \infty) = \frac{1}{\omega^+} + \frac{Un}{2\omega^{+2}} + \sum_{\vec{k}} \frac{-V_{\vec{k}}^2 + U^2 n/2}{\omega^{+3}}$$

$$G_{12}(\omega \to \infty)) = \frac{U\Phi}{\omega^{+2}} + \frac{U^2\Phi}{\omega^{+3}}$$

$$(A.60)$$

Non-interacting Green's function in high frequency limit is given by

$$\hat{\mathscr{G}}_0(\omega \to \infty) = \omega^+ - \sum_{\vec{k}} V_{\vec{k}}^2 / \omega^+ \sigma_z \qquad (A.61)$$

Self-energy in high frequency limit is given by

$$\hat{\Sigma}(\omega \to \infty) = \hat{\mathscr{G}}_0^{-1}(\omega \to \infty) - \hat{G}^{-1}(\omega \to \infty) \qquad (A.62)$$

$$\Sigma_{11}(\omega \to \infty) = \omega - \sum_{\vec{k}} V_{\vec{k}}^2/\omega - \frac{1/\omega + Un/(2\omega^2) + (-\sum_{\vec{k}} V_{\vec{k}}^2 + U^2 n/2)/\omega^3}{1/\omega^2 - U^2 n^2/(4\omega^4) - U^2 \Phi^2/\omega^4}$$

$$= \omega - \sum_{\vec{k}} V_{\vec{k}}^2/\omega - [1/\omega + Un/(2\omega^2) + (-\sum_{\vec{k}} V_{\vec{k}}^2 + U^2 n/2)/\omega^3]\omega^2[1 - U^2 n^2/(4\omega^2) - U^2 \Phi^2/\omega^2]^{-1}$$

$$= \omega - \sum_{\vec{k}} V_{\vec{k}}^2/\omega - [1/\omega + Un/(2\omega^2) + (-\sum_{\vec{k}} V_{\vec{k}}^2 + U^2 n/2)/\omega^3]\omega^2[1 + U^2 n^2/(4\omega^2) + U^2 \Phi^2/\omega^2]$$

$$= \omega - \sum_{\vec{k}} V_{\vec{k}}^2/\omega - [\omega + Un/2 - \sum_{\vec{k}} (V_{\vec{k}}^2 + U^2 n/2)/\omega][1 + U^2 n^2/(4\omega^2) + U^2 \Phi^2/\omega^2]$$

$$= \omega - \sum_{\vec{k}} V_{\vec{k}}^2/\omega - [\omega + Un/2 - \sum_{\vec{k}} (V_{\vec{k}}^2 + U^2 n/2)/\omega + U^2 n^2/(4\omega) + U^2 \Phi^2/\omega]$$

$$= -Un/2 + U^2 n/(2\omega) - U^2 n^2/(4\omega) - U^2 \Phi^2/\omega$$

$$(A.63)$$

Taking $\frac{1}{\omega^n} \to 0$, where $n \geq 2$.

Thus A_{11} is given by

$$-Un/2 + U^2 n/(2\omega) - U^2 n^2/(4\omega) - U^2 \Phi^2/\omega = -Un/2 + A_{11}\frac{U^2}{\omega^+}\left[\frac{n_0}{2} - \frac{n_0^2}{4} - \Phi_0^2\right]$$

$$A_{11} = \frac{U^2 n/2 - U^2 n^2/4 - U^2 \Phi^2}{U^2 n_0/2 - U^2 n_0^2/4 - U^2 \Phi_0^2} \quad (A.64)$$

Similarly one can find, $A_{11} = A_{22}$.

A.5 Fermions in high dimensions

A.5.1 Effective action of repulsive Hubbard model

Let us consider repulsive Hubbard model.

$$\mathcal{H} = \varepsilon_f \sum_{i\sigma} c_{i\sigma}^\dagger c_{i\sigma} - \sum_{<ij\sigma>} [t_{ij} c_{i\sigma}^\dagger c_{j\sigma} + h.c] + U \sum_i n_{i\uparrow} n_{i\downarrow} - \mu \sum_{i\sigma} c_{i\sigma}^\dagger c_{i\sigma} \qquad (A.65)$$

Then, action of Hubbard model is given by

$$S\{c_i^*, c_i\} = \int_0^\beta d\tau \left[\sum_{i\sigma} c_{i\sigma}^*(\tau) \left(\frac{\partial}{\partial \tau} - \mu + \varepsilon_f \right) c_{i\sigma}(\tau) - \sum_{<ij\sigma>} t_{ij} c_{i\sigma}^*(\tau) c_{j\sigma}(\tau) + \right.$$
$$\left. U \sum_i c_{i\uparrow}^*(\tau) c_{i\uparrow}(\tau) c_{i\downarrow}^*(\tau) c_{i\downarrow}(\tau) \right] \tag{A.66}$$

where c_i^* and c_i are Grassmann numbers. The partition function of system is given by

$$\mathscr{Z} = \int \prod_{i\sigma} \mathscr{D} c_{i\sigma}^* \mathscr{D} c_{i\sigma} \exp(-S\{c_i^*, c_i\}) \tag{A.67}$$

We can write action as

$$S = S_o + \Delta S + S^{(o)} \tag{A.68}$$

Where S_o contains variables on site o and is given by

$$S_o = \int_0^\beta d\tau \left[\sum_\sigma c_{o\sigma}^*(\tau) \left(\frac{\partial}{\partial \tau} - \mu + \varepsilon_f \right) c_{o\sigma}(\tau) + \right.$$
$$\left. U c_{o\uparrow}^*(\tau) c_{o\uparrow}(\tau) c_{o\downarrow}^*(\tau) c_{o\downarrow}(\tau) \right] \tag{A.69}$$

ΔS contains the hopping between site o and other sites of the lattice and is given by

$$\Delta S = - \int_0^\beta \sum_{j\sigma} [t_{oj} c_{o\sigma}^*(\tau) c_{j\sigma}(\tau) + h.c] \tag{A.70}$$

$S^{(o)}$ contains all site variables except o and is given by

$$S^{(o)} = \int_0^\beta d\tau \left[\sum_{i\sigma \neq o} c_{i\sigma}^*(\tau) \left(\frac{\partial}{\partial \tau} - \mu + \varepsilon_f \right) c_{i\sigma}(\tau) - \sum_{<ij\sigma \neq o>} t_{ij} c_{i\sigma}^*(\tau) c_{j\sigma}(\tau) + \right.$$
$$\left. U \sum_{i \neq o} c_{i\uparrow}^*(\tau) c_{i\uparrow}(\tau) c_{i\downarrow}^*(\tau) c_{i\downarrow}(\tau) \right] \tag{A.71}$$

The partition function is given by

$$\mathscr{Z} = \int \prod_{i\sigma} \mathscr{D}c_{i\sigma}^* \mathscr{D}c_{i\sigma} \exp(-[S_o\{c_o^*, c_o\} + \Delta S\{c_i^*, c_i, c_o^*, c_o\} +$$

$$S^{(o)}\{c_{i\neq o}^*, c_{i\neq o}\}]) \tag{A.72}$$

Now by integrating over all lattice degree of freedom except o, we can write partition function as

$$\mathscr{Z} = \int \prod_{\sigma} \mathscr{D}c_{o\sigma}^* \mathscr{D}c_{o\sigma} exp\{-S_o[c_{o\sigma}, c_{o,\sigma}^*]\} \int \prod_{i\sigma\neq 0} \mathscr{D}c_{i\sigma}^* \mathscr{D}c_{i\sigma}$$

$$exp[-S^{(o)}\{c_{i\neq o}^*, c_{i\neq o}\}] exp[-\Delta S\{c_i^*, c_i, c_o^*, c_o\}] \tag{A.73}$$

The partition function of system when site o is removed is given by.

$$\mathscr{Z}^{(o)} = \int \prod_{i\sigma\neq 0} \mathscr{D}c_{i\sigma}^* \mathscr{D}c_{i\sigma} exp[-S^{(o)}\{c_{i\neq o\sigma}^*, c_{i\neq o\sigma}\}] \tag{A.74}$$

Then we can write equation (A.72) as

$$\mathscr{Z} = \mathscr{Z}^{(o)} \int \prod_{\sigma} \mathscr{D}c_{o\sigma}^* \mathscr{D}c_{o\sigma} exp\{-S_o[c_{o\sigma}, c_{o,\sigma}^*]\}$$

$$\langle exp[-\Delta S\{c_i^*, c_i, c_o^*, c_o\}]\rangle_{(o)} \tag{A.75}$$

Where $\langle ....\rangle_{(o)}$ is average over the ensemble when site o is removed. Since in above Hamiltonian, the number is conserved so if an operator $\hat{A}$ does not have equal number of $c_{i\sigma}$ and $c_{i\sigma}^*$ then $\langle\hat{A}\rangle_{(o)}$ will vanish. Thus $\langle \exp(-\Delta S)\rangle_{(o)}$ is given by

$$\langle \exp(-\Delta S)\rangle_{(o)} = \langle 1 - \Delta S + \frac{1}{2!}(\Delta S)^2 - ...\rangle_{(o)} \tag{A.76}$$

$$\langle \Delta S\rangle_{(o)} = 0 \tag{A.77}$$

Because it does not contain equal number of $c_{i\sigma}$ and $c_{i\sigma}^*$. Now the second order term is given by

$$< (\Delta S)^2 >_{(o)} = \int_0^\beta d\tau_1 \int_0^\beta d\tau_2 \sum_\sigma \sum_{jk \neq o} [t_{jo} t_{ok} \langle c_{j\sigma}^*(\tau_1) c_{o\sigma}(\tau_1) c_{o\sigma}^*(\tau_2) c_{k\sigma}(\tau_2) \rangle_{(o)} +$$

$$t_{ko} t_{oj} \langle c_{o\sigma}^*(\tau_1) c_{j\sigma}(\tau_1) c_{k\sigma}^*(\tau_2) c_{o\sigma}(\tau_2) \rangle_{(o)}] \qquad (A.78)$$

First term is written as

$$t_{jo} t_{ok} \langle c_{j\sigma}^*(\tau_1) c_{o\sigma}(\tau_1) c_{o\sigma}^*(\tau_2) c_{k\sigma}(\tau_2) \rangle_{(o)} =$$

$$t_{jo} t_{ok} \langle c_{o\sigma}^*(\tau_2) c_{k\sigma}(\tau_2) c_{j\sigma}^*(\tau_1) c_{j\sigma}(\tau_1) \rangle_{(o)} \qquad (A.79)$$

The cavity Green's function is given by

$$G_{jk\sigma}^{(o)}(\tau_1 - \tau_2) = -\langle T_\tau c_{j\sigma}(\tau_1) c_{k\sigma}^*(\tau_2) \rangle_{(o)}, \qquad (A.80)$$

where T_τ is time ordering operator. Now we can write equation (A.78) in term of one particle Green's function.

$$< (\Delta S)^2 >_{(o)} = -\int_0^\beta d\tau_1 \int_0^\beta d\tau_2 \sum_\sigma \sum_{jk \neq o} [t_{jo} t_{ok} G_{jk\sigma}^{(o)}(\tau_1 - \tau_2)$$

$$c_{o\sigma}^*(\tau_1) c_{o\sigma}(\tau_2)] \qquad (A.81)$$

Higher order term can be obtained in similar way by using higher order Green's function. The effective action in term of higher order Green's function is given by

$$S_{eff}(o) = S_o + \sum_{n=1}^\infty \sum_{i_1, i_2 \ldots, j_1, j_2 \ldots, j_n} \int d\tau_{i_1} \ldots d\tau_{i_n} d\tau_{j_1} \ldots d\tau_{j_n} t_{i_1 o} \ldots t_{i_n o} t_{o j_1} \ldots t_{o j_n} c_{o\sigma}^*(\tau_{i_1}) \ldots$$

$$c_{o\sigma}^*(\tau_{i_n}) c_{o\sigma}(\tau_{j_1}) \ldots c_{o\sigma}(\tau_{j_n}) G_{i_1 \ldots, i_n, j_1 \ldots, j_n}^{(o)}(\tau_{i_1} \ldots, \tau_{i_n}, \tau_{j_1} \ldots, \tau_{j_n}) \qquad (A.82)$$

A.6   Infinite dimensional limit

A.6.1   Scaling of hopping in infinite dimension

The non-interacting density of state in d-dimension is given by

$$N(E) = \sum_{\vec{k}} \delta(E - \varepsilon_{\vec{k}}) \tag{A.83}$$

Where $\vec{k}$ is d-dimensional wave vector, $\varepsilon_{\vec{k}}$ is dispersion relation and is given by

$$\varepsilon_{\vec{k}} = -2t \sum_{i=1}^{d} cos(k_i) \tag{A.84}$$

In infinite dimension we can think of $cos(k_i)$ distributed between -1 to 1 randomly with uniform probability distribution $P(k_i) = 1.0/\pi$ for all $k_i \in [-\pi/2, \pi/2]$. Then first and second moments of $\varepsilon_{\vec{k}}$ are given by

$$\langle \varepsilon_{\vec{k}} \rangle = -2t \sum_{i=1}^{d} \int_{-\pi/2}^{\pi/2} P(k_i) cos(k_i) dk_i = 0 \tag{A.85}$$

$$\langle \varepsilon_{\vec{k}}^2 \rangle = 4t^2 \sum_{i,j=1}^{d} \int_{-\pi/2}^{\pi/2} P(k_i) cos(k_i) cos(k_j) dk_i$$

$$= 4t^2 \sum_{i=1}^{d} \int_{-\pi/2}^{\pi/2} \frac{1}{\pi} cos(k_i) cos(k_i) dk_i = 2dt^2 \tag{A.86}$$

According to central limit theorem, in $d \to \infty$ the distribution function of sum of equation A.84 should be Gaussian, and probability of finding a state ε_k is density of state ($N(E)$). Thus $N(E)$ is given by

$$N(E) = \frac{1}{\sqrt{2\pi \langle \varepsilon_k^2 \rangle - \langle \varepsilon_k \rangle^2}} exp^{-\frac{(E - \langle \varepsilon_k \rangle)^2}{2(\langle \varepsilon_k^2 \rangle - \langle \varepsilon_k \rangle^2)}}$$

$$= \frac{1}{\sqrt{4\pi dt^2}} exp^{-\frac{E^2}{4dt^2}} \tag{A.87}$$

For d$\rightarrow \infty$, $N(E)$ is featureless, thus t must scale properly. $2dt^2 = t^*$, where t^* is scaled hopping, a constant number.

$$N(E) = \frac{1}{\sqrt{2\pi t^{*2}}} exp^{-\frac{E^2}{2t^{*2}}} \tag{A.88}$$

Thus in infinite dimension hopping t scaled like $t \rightarrow t^*/\sqrt{2d}$.

As we know that $\langle c_k^\dagger c_j \rangle$ is probability amplitude of electron to hop from site j to k. For nearest neighbour hopping $|\langle c_k^\dagger c_j \rangle|^2$ will be directly proportional to inverse of coordination number ($q = 2d$), thus single particle Green's function scaled like $G_{jk} \rightarrow 1/\sqrt{d}$. For arbitrary j, k, $G_{jk} \rightarrow d^{-||j-k||/2}$ [2]. In order to calculate the summation involving n-connected Green's function , we have to determine the overall scaling factor. Let us focus on first term which contains single particle Green's function. We find a contribution d^2 from summation over i and j, d^{-1} from t^2, and d^{-1} from G_{ij}, that gives net constant scaling factor. For second term, we find a contribution d^4 from summation over four indices, contribution d^{-2} from hopping and contribution d^{-3} from G_{i_1,i_2,j_1,j_2}, thus second term scale as $1/d$, and it vanishes as $d \rightarrow \infty$. Therefore, it can be seen that higher order term will vanish in infinite dimension and only first term contribute.

In infinite dimension as $d \rightarrow \infty$ the partition can be written using Linked Cluster Theorem as

$$\begin{aligned}
\mathscr{Z} = \ & \mathscr{Z}^{(o)} \int \prod_\sigma \mathscr{D}c_{o\sigma}^* \mathscr{D}c_{o\sigma} \exp\{-S_o[c_{o\sigma}, c_{o,\sigma}^*]\} \\
& \exp\left[-\int_0^\beta d\tau_1 \int_0^\beta d\tau_2 \sum_\sigma \sum_{jk \neq o} [t_{jo}^* t_{ok}^* G_{jk\sigma}^{(o)}(\tau_1 - \tau_2) c_{o\sigma}^*(\tau_1) c_{o\sigma}(\tau_2)] \right]
\end{aligned} \tag{A.89}$$

where t_{jo}^* is scaled hopping. From equation A.89, it is clear that the full partition function is a product of two terms: the partition function when o site is removed and other which contain all the effects of sites other than the site o. So from equation A.89 effective action of site o is given by

$$S^{eff}(o) = S_o[c_{o\sigma}, c_{o,\sigma}^*] + \int_0^\beta d\tau_1 \int_0^\beta d\tau_2 \sum_\sigma \sum_{jk \neq o} [t_{jo}^* t_{ok}^* G_{jk\sigma}(\tau_1 - \tau_2)] c_{o\sigma}^*(\tau_1) c_{o\sigma}(\tau_2)] \tag{A.90}$$

We can write equation A.90 as

$$S^{eff}(o) = S_o[c_{o\sigma}, c^*_{o,\sigma}] + \int_0^\beta d\tau_1 \int_0^\beta d\tau_2 \sum_\sigma \sum_{jk \neq o} [t^*_{jo} t^*_{ok} G_{jk\sigma}(\tau_1 - \tau_2)] c^*_{o\sigma}(\tau_1) c_{o\sigma}(\tau_2)] \tag{A.91}$$

From equation A.91 it is clear that site o is coupled with a mean field which contain the effect of other lattice site on site o. This field is also depending on time. The mean field is given by

$$\Delta_\sigma(\tau_1 - \tau_2) = -\sum_\sigma \sum_{jk \neq o} [t^*_{jo} t^*_{ok} G_{jk\sigma}(\tau_1 - \tau_2)] \tag{A.92}$$

Now let us define a non-interacting mean field propagator $\mathscr{G}_\sigma$.

$$\mathscr{G}_\sigma^{-1}(\tau_1 - \tau_2) = -\left(\frac{\partial}{\partial \tau_1} - \mu + \varepsilon_f\right)\delta_{\tau_1 \tau_2} - \Delta_\sigma(\tau_1 - \tau_2) \tag{A.93}$$

$$S^{eff}(o) = -\int_0^\beta d\tau_1 \int_0^\beta d\tau_2 \sum_\sigma c^*_{o\sigma}(\tau_1)\mathscr{G}_\sigma^{-1}(\tau_1 - \tau_2)c_{o\sigma}(\tau_2) + U \int_0^\beta d\tau c^*_{o\uparrow}(\tau)$$
$$c_{o\uparrow}(\tau)c^*_{o\downarrow}(\tau)c_{o\downarrow}(\tau) \tag{A.94}$$

A.6.2 Effective action of attractive Hubbard model

The attractive Hubbard model is given by

$$\mathscr{H} = \varepsilon_f \sum_{i\sigma} c^\dagger_{i\sigma}c_{i\sigma} - \sum_{<ij\sigma>} [t_{ij}c^\dagger_{i\sigma}c_{j\sigma} + h.c] - U \sum_i n_{i\uparrow}n_{i\downarrow} - \mu \sum_{i\sigma} c^\dagger_{i\sigma}c_{i\sigma} \tag{A.95}$$

Then, action of Hubbard model in Nambu formulation is given by is given by

$$S\{c^*_i, c_i\} = \int_0^\beta d\tau \left[\sum_{i\sigma} \Psi^*_i(\tau)\left(\frac{\partial}{\partial \tau} + (-\mu + \varepsilon_f)\sigma_z\right)\Psi_i(\tau) - \sum_{<ij\sigma>} t_{ij}c^*_{i\sigma}(\tau)c_{j\sigma}(\tau) - \right.$$
$$\left. U \sum_i c^*_{i\uparrow}(\tau)c_{i\uparrow}(\tau)c^*_{i\downarrow}(\tau)c_{i\downarrow}(\tau) \right] \tag{A.96}$$

where Ψ is two component Nambu spinor and is given by

$$\Psi_i(\tau) = \begin{bmatrix} c_{i\uparrow}(\tau) \\ c_{i\downarrow}^*(\tau) \end{bmatrix}$$

Now divide action into three parts

$$S = S_o + \Delta S + S^{(o)} \tag{A.97}$$

Where S_o contains variables on site o, and is given by

$$S_o = \int_0^\beta d\tau \left[\sum_\sigma \Psi_o^*(\tau) \left(\frac{\partial}{\partial \tau} + (-\mu + \varepsilon_f)\sigma_z \right) \Psi_o(\tau) - U c_{o\uparrow}^*(\tau) c_{o\uparrow}(\tau) c_{o\downarrow}^*(\tau) c_{o\downarrow}(\tau) \right] \tag{A.98}$$

ΔS contains the hopping between site o and other sites of the lattice, and is given by

$$\Delta S = -\int_0^\beta \sum_{j\sigma} [t_{oj} c_{o\sigma}^*(\tau) c_{j\sigma}(\tau) + h.c] \tag{A.99}$$

$S^{(o)}$ contains all site variables except o, and is given by

$$S^{(o)} = \int_0^\beta d\tau \left[\sum_{i\sigma \neq o} \Psi_i^*(\tau) \left(\frac{\partial}{\partial \tau} + (-\mu + \varepsilon_f)\sigma_z \right) \Psi_i(\tau) - \sum_{<ij\sigma \neq o>} t_{ij} c_{i\sigma}^*(\tau) c_{j\sigma}(\tau) - \right.$$
$$\left. U \sum_{i \neq o} c_{i\uparrow}^*(\tau) c_{i\uparrow}(\tau) c_{i\downarrow}^*(\tau) c_{i\downarrow}(\tau) \right] \tag{A.100}$$

The partition function is given by

$$\mathscr{Z} = \int \prod_{i\sigma} \mathscr{D}c_{i\sigma}^* \mathscr{D}c_{i\sigma} \exp(-[S_o\{c_o^*, c_o\} + \Delta S\{c_i^*, c_i, c_o^*, c_o\} + S^{(o)}\{c_{i\neq o}^*, c_{i\neq o}\}]) \tag{A.101}$$

$$\mathscr{Z} = \mathscr{Z}^{(o)} \int \prod_\sigma \mathscr{D}c_{o\sigma}^* \mathscr{D}c_{o\sigma} exp\{-S_o[c_{o\sigma}, c_{o,\sigma}^*]\}$$
$$\langle exp[-\Delta S\{c_i^*, c_i, c_o^*, c_o\}] \rangle_{(o)} \tag{A.102}$$

Where $\langle....\rangle_{(o)}$ is average over the ensemble when site o is removed. Thus $\langle\exp(-\Delta S)\rangle_{(o)}$ is given by

$$\langle\exp(-\Delta S)\rangle_{(o)} = \langle 1 - \Delta S + \frac{1}{2!}(\Delta S)^2 - ...\rangle_{(o)} \tag{A.103}$$

$$\langle\Delta S\rangle_{(o)} = 0 \tag{A.104}$$

Now the second order, non-vanishing terms are given by

$$\langle(\Delta S)^2\rangle_{(o)} = \langle\int_0^\beta d\tau_1 \int_0^\beta d\tau_2 \sum_{jk\neq o\sigma_1\sigma_2} t_{jo}t_{ok}[c^*_{o\sigma_1}(\tau_1)c_{j\sigma_1}(\tau_1)c^*_{o\sigma_2}(\tau_2)c_{k\sigma_2}(\tau_2) +$$
$$c^*_{o\sigma_1}(\tau_1)c_{j\sigma_1}(\tau_1)c^*_{k\sigma_2}(\tau_2)c_{o\sigma_2}(\tau_2) + c^*_{j\sigma_1}(\tau_1)c_{o\sigma_1}(\tau_1))c^*_{o\sigma_2}(\tau_2)c_{k\sigma_2}(\tau_2) +$$
$$c^*_{j\sigma_1}(\tau_1)c_{o\sigma_1}(\tau_1)c^*_{k\sigma_2}(\tau_2)c_{o\sigma_2}(\tau_2)]\rangle_{(o)} \tag{A.105}$$

Then non-vanishing terms are given by

$$\langle(\Delta S)^2\rangle_{(o)} = \langle\int_0^\beta d\tau_1 \int_0^\beta d\tau_2 \sum_{jk\neq o} t_{jo}t_{ok}[c^*_{o\uparrow}(\tau_1)c_{j\uparrow}(\tau_1)c^*_{o\downarrow}(\tau_2)c_{k\downarrow}(\tau_2) +$$
$$c^*_{o\downarrow}(\tau_1)c_{j\downarrow}(\tau_1)c^*_{o\uparrow}(\tau_2)c_{k\uparrow}(\tau_2) + c^*_{o\uparrow}(\tau_1)c_{j\uparrow}(\tau_1)c^*_{k\uparrow}(\tau_2)c_{o\uparrow}(\tau_2) +$$
$$c^*_{o\downarrow}(\tau_1)c_{j\downarrow}(\tau_1)c^*_{k\downarrow}(\tau_2)c_{o\downarrow}(\tau_2) + c^*_{j\uparrow}(\tau_1)c_{o\uparrow}(\tau_1))c^*_{o\uparrow}(\tau_2)c_{k\uparrow}(\tau_2) + c^*_{j\downarrow}(\tau_1)c_{o\downarrow}(\tau_1))c^*_{o\downarrow}(\tau_2)c_{k\downarrow}(\tau_2) +$$
$$c^*_{j\uparrow}(\tau_1)c_{o\uparrow}(\tau_1)c^*_{k\downarrow}(\tau_2)c_{o\downarrow}(\tau_2) + c^*_{j\downarrow}(\tau_1)c_{o\downarrow}(\tau_1)c^*_{k\uparrow}(\tau_2)c_{o\uparrow}(\tau_2)]\rangle_{(o)} \tag{A.106}$$

$$\langle(\Delta S)^2\rangle_{(o)} = \int_0^\beta d\tau_1 \int_0^\beta d\tau_2 \sum_{jk\neq o} t_{jo}t_{ok}[-c^*_{o\uparrow}(\tau_1)\langle c_{j\uparrow}(\tau_1)c_{k\downarrow}(\tau_2)\rangle c^*_{o\downarrow} -$$
$$c^*_{o\downarrow}(\tau_1)\langle c_{j\downarrow}(\tau_1)c_{k\uparrow}(\tau_2)\rangle c^*_{o\uparrow}(\tau_2) + c^*_{o\uparrow}(\tau_1)\langle c_{j\uparrow}(\tau_1)c^*_{k\uparrow}(\tau_2)\rangle c_{o\uparrow}(\tau_2) + c^*_{o\downarrow}(\tau_1)\langle c_{j\downarrow}(\tau_1)c^*_{k\downarrow}(\tau_2)\rangle c_{o\downarrow}(\tau_2) +$$
$$c_{o\uparrow}(\tau_1))\langle c^*_{j\uparrow}(\tau_1)c_{k\uparrow}(\tau_2)\rangle c^*_{o\uparrow}(\tau_2) + c_{o\downarrow}(\tau_1))\langle c^*_{j\downarrow}(\tau_1)c_{k\downarrow}(\tau_2)\rangle c^*_{o\downarrow}(\tau_2) -$$
$$c_{o\uparrow}(\tau_1)\langle c^*_{j\uparrow}(\tau_1)c^*_{k\downarrow}(\tau_2)\rangle c_{k\downarrow}(\tau_2) - c_{o\downarrow}(\tau_1)\langle c^*_{j\downarrow}(\tau_1)c^*_{k\uparrow}(\tau_2)\rangle c_{o\uparrow}(\tau_2)] \tag{A.107}$$

Now introduce normal and anomalous cavity Green's function

$$
\begin{aligned}
G^{11}_{jk}(\tau_1 - \tau_2) &= -\langle T_\tau c_{k\uparrow}(\tau_1) c^*_{j\uparrow}(\tau_2)\rangle_{(o)} \\
G^{12}_{jk}(\tau_1 - \tau_2) &= -\langle T_\tau c_{k\uparrow}(\tau_1) c_{j\downarrow}(\tau_2)\rangle_{(o)} \\
G^{21}_{jk}(\tau_1 - \tau_2) &= -\langle T_\tau c^*_{k\downarrow}(\tau_1) c^*_{j\uparrow}(\tau_2)\rangle_{(o)} \\
G^{22}_{jk}(\tau_1 - \tau_2) &= -\langle T_\tau c^*_{k\downarrow}(\tau_1) c_{j\downarrow}(\tau_2)\rangle_{(o)}
\end{aligned}
\tag{A.108}
$$

$$
\begin{aligned}
\langle(\Delta S)^2\rangle_{(o)} = \int_0^\beta d\tau_1 \int_0^\beta d\tau_2 \sum_{jk\neq o} t_{jo}t_{ok} 2[c^*_{o\uparrow}(\tau_1) G^{12}_{jk}(\tau_1-\tau_2) c^*_{o\downarrow} - \\
c^*_{o\uparrow}(\tau_1) G^{11}_{jk}(\tau_1-\tau_2) c_{o\uparrow}(\tau_2) - c_{o\downarrow}(\tau_1)) G^{22}_{jk}(\tau_1-\tau_2) c^*_{o\downarrow}(\tau_2) - \\
c_{o\downarrow}(\tau_1) G^{21}_{jk}(\tau_1-\tau_2) c_{o\uparrow}(\tau_2)]
\end{aligned}
\tag{A.109}
$$

Now define hybridisation function matrix $\hat{\Delta}(\tau_1 - \tau_2)$

$$
\begin{aligned}
\Delta^{11}(\tau_1 - \tau_2) &= -\sum_{jk\neq o} t_{jo}t_{ok} G^{11}_{jk}(\tau_1-\tau_2) \\
\Delta^{12}(\tau_1 - \tau_2) &= \sum_{jk\neq o} t_{jo}t_{ok} G^{12}_{jk}(\tau_1-\tau_2) \\
\Delta^{21}(\tau_1 - \tau_2) &= \sum_{jk\neq o} t_{jo}t_{ok} G^{21}_{jk}(\tau_1-\tau_2) \\
\Delta^{22}(\tau_1 - \tau_2) &= -\sum_{jk\neq o} t_{jo}t_{ok} G^{22}_{jk}(\tau_1-\tau_2)
\end{aligned}
\tag{A.110}
$$

Higher order term will vanish in infinite dimension thus effective action is given by

$$
S_{eff}(o) = -\int_0^\beta d\tau_1 d\tau_2 \left[\Psi^*(\tau_1)\left((-\frac{\partial}{\partial\tau} + (\mu - \varepsilon_f)\sigma_z)\delta_{\tau_1\tau_2} - \hat{\Delta}(\tau_1-\tau_2)\right)\Psi(\tau_2)\right] -
$$
$$
\int_0^\beta d\tau\, U c^*_\uparrow(\tau) c_\uparrow(\tau) c^*_\downarrow(\tau) c_\downarrow(\tau) \tag{A.111}
$$

Bibliography

[1] Georges A, Giamarchi T 2013 arXiv:1308.2684.

[2] Vollhardt D AIP Conference Proceedings 2010 **1297** 339.